IBNORM: INFORMATION-BOTTLENECK INSPIRED NORMALIZATION FOR REPRESENTATION LEARNING

Xiandong ZouSingapore Management University

Pan Zhou *
Singapore Management University

ABSTRACT

Normalization is fundamental to deep learning, but existing approaches such as BatchNorm, LayerNorm, and RMSNorm are variance-centric by enforcing zero mean and unit variance, stabilizing training without controlling how representations capture task-relevant information. We propose IB-Inspired Normalization (IBNorm), a simple yet powerful family of methods grounded in the Information Bottleneck principle. IBNorm introduces bounded compression operations that encourage embeddings to preserve predictive information while suppressing nuisance variability, yielding more informative representations while retaining the stability and compatibility of standard normalization. Theoretically, we prove that IBNorm achieves a higher IB value and tighter generalization bounds than variance-centric methods. Empirically, IBNorm consistently outperforms Batch-Norm, LayerNorm, and RMSNorm across large-scale language models (LLaMA, GPT-2) and vision models (ResNet, ViT), with mutual information analysis confirming superior information bottleneck behavior. Code will be released publicly.

1 Introduction

Normalization has become a cornerstone of deep learning, credited for stabilizing and accelerating training across domains. Techniques such as Batch Normalization (BN) (Ioffe & Szegedy, 2015), Layer Normalization (LN) (Ba et al., 2016), and RMSNorm (Zhang & Sennrich, 2019) are now standard in architectures spanning vision and language (Vaswani et al., 2017; Dosovitskiy et al., 2020; He et al., 2016a), underscoring normalization as a key driver of training stability and acceleration.

Despite this success, existing normalization methods share a fundamental limitation: they are inherently *variance-centric*. By enforcing zero mean and unit variance, followed by rescaling and shifting, they improve the conditioning of the optimization problem (Huang et al., 2023; 2018; He et al., 2016b; Desjardins et al., 2015). However, this process operates purely on first- and second-order statistics, without offering any guidance on (intermediate) representation learning. Indeed, two representations may share identical mean and variance, but can encode drastically different amounts of task-relevant information. This raises a key question: can normalization be re-designed not only to stabilize training but also to shape representations toward sufficiency and generalization?

Early attempts have explored this direction. For instance, Eftekhari & Papyan (2025) encouraged Gaussian-like features via power transforms and additive noise, arguing that Gaussianity aids representation and noise acts as implicit regularization. However, such approaches lack a principled information-theoretic foundation and fail to explicitly balance preserving predictive information against suppressing nuisance factors, often yielding suboptimal embeddings for downstream tasks.

Contributions. In this work, we move beyond variance-centric normalization and introduce **IB-Norm**, a simple yet powerful normalization method grounded by the Information Bottleneck (IB) principle (Shamir et al., 2010; Tishby & Zaslavsky, 2015; Shwartz-Ziv & Tishby, 2017). Moreover, we also theoretically justify the superiority of IBNorm and its better generalization performance.

First, we introduce an IB perspective to normalization, and propose IBNorm for generalization improvement. The IB principle seeks representations that preserve task-relevant information while discarding nuisances, thereby connecting normalization to generalization. Within this framework, we decompose existing normalization methods into three steps: (i) grouping features (e.g., across

^{*}Corresponding author.

batch, channel, or dimension), (ii) standardization, and (iii) recovery via re-scaling and shifting. Our analysis reveals that the normalization operation itself is the key bottleneck governing information flow. Building on this insight, IBNorm (IBNorm-S, IBNorm-L, IBNorm-T) introduces compression operators that selectively compress activations toward their means, providing explicit control over sufficiency—redundancy tradeoffs while remaining drop-in compatible with existing architectures.

Second, we provide theoretical guarantees. Under the IB framework, we prove that IBNorm achieves a strictly larger IB value than variance-centric methods like LN and BN, thereby better balancing predictive sufficiency with nuisance suppression. Moreover, we establish a provably tighter generalization bound, explaining why IBNorm consistently outperforms standard normalization in practice.

Extensive experiments show the effectiveness of IBNorm across architectures and modalities. In language modeling, integrating IBNorm into LLaMA (Touvron et al., 2023b) and GPT-2 (Radford et al., 2019) consistently outperforms LN, RMSNorm, and NormalNorm on LLM Leaderboard I/II by up to 8.75%. In vision, applying IBNorm to ResNet (He et al., 2016a) and ViT (Dosovitskiy et al., 2020) yields substantial gains, e.g., 3.98% improvement on ImageNet (Deng et al., 2009) (ResNet-50), and up to 8.17% improvement on ImageNet (ViT).

2 RELATED WORK

Normalization plays a central role in modern deep learning, enabling faster convergence and improved generalization across natural language processing (NLP) (Devlin et al., 2019; Vaswani et al., 2017; Touvron et al., 2023a;b; Dubey et al., 2024; Bai et al., 2023; Liu et al., 2024) and computer vision (CV) (He et al., 2016a; Dosovitskiy et al., 2020; Liu et al., 2022).

Batch Normalization (BN) (Ioffe & Szegedy, 2015) normalizes activations across mini-batches to stabilize training, with numerous extensions such as Mean-only BN (Salimans & Kingma, 2016), L^p -Norm BN (Liao et al., 2016), Conditional BN (De Vries et al., 2017), and Whitening BN (Siarohin et al., 2018). Layer Normalization (LN) (Ba et al., 2016) was proposed for sequential and small-batch settings and has inspired variants including Dynamic LN (Kim et al., 2017), RM-SNorm (Zhang & Sennrich, 2019), and Adaptive LN (Xu et al., 2019), which are now standard in Transformers (Vaswani et al., 2017; Dosovitskiy et al., 2020). Group Normalization (GN) (Wu & He, 2018) and Batch Group Normalization (BGN) (Summers & Dinneen, 2019) extend this idea by combining grouping across features, channels, or batches. Collectively, these methods underscore normalization as a structural tool for scaling depth and stabilizing optimization.

Beyond variance-centric approaches, some works attempt to explicitly shape activation distributions. For example, Eftekhari & Papyan (2025) encourage Gaussian-like features via power transforms with additive noise, arguing that Gaussianity enhances representational capacity while noise acts as implicit regularization. However, this approach faces key limitations: it does not optimize mutual information with targets, incurs overhead in estimating power parameters, and introduces stochasticity that can destabilize training (see Appendix B).

Broadly, most normalization methods rely on re-centering and rescaling to mitigate internal covariate shift, yet they overlook the information-theoretic properties of representations, such as sufficiency and redundancy. This gap motivates our work. We propose **IBNorm**, which augments conventional normalization with compression operation designed to regulate information flow, guiding activations toward IB-optimal representations that enhance both generalization and robustness.

3 Preliminary

Here we introduce information bottleneck (IB) framework (Tishby et al., 2000; Shamir et al., 2010; Tishby & Zaslavsky, 2015) which forms the basis of our approach in Sec. 4.

Consider two continuous random variables X and Y with joint probability densities p(x,y) over the space $\mathcal{X} \times \mathcal{Y}$. Then, we can define the mutual information between X and Y:

$$I(X;Y) = \int_{x \in \mathcal{X}} \int_{y \in \mathcal{Y}} p(x,y) \log \frac{p(x,y)}{p(x) p(y)} dx dy.$$
 (1)

Mutual information measures dependencies between random variables, and can be understood as how much knowing X reduces the uncertainty in Y or vice versa.

Building on this, the IB framework formulates representation learning as a trade-off between two goals: 1) minimality which compresses X by reducing I(X;T); and 2) sufficiency which preserves information about Y by maximizing I(Y;T). This is captured by the IB objective (Tishby & Zaslavsky, 2015):

 $\max_{T} \left[I(Y;T) - \beta I(X;T) \right]. \tag{2}$

where $\beta > 0$. Here, T must satisfy the Markov chain T - X - Y, and the optimal representation T^* is given by the conditional distribution $p_{T^*|X}(t|x)$ with marginal $p_{T^*}(t) = \int p_{T^*|X}(t|x)p_X(x)dx$ govern by self-consistency equations (Tishby et al., 2000; Shamir et al., 2010).

Intuitively, maximizing I(Y;T) ensures that the representation T preserving all information relevant for predicting the target variable Y, thereby enhancing predictive power and interpretability. Concurrently, penalizing I(X;T) enforces compression, which eliminates irrelevant variability in the representation and, in turn, enhances generalization and robustness of the representation (Kawaguchi et al., 2023; Alemi et al., 2016; Goldfeld & Polyanskiy, 2020; Saxe et al., 2019; Federici et al., 2020).

4 METHODOLOGY

Inspired by the IB principle introduced in Sec. 3, we now present how it motivates a novel and more effective normalization strategy — an essential component of modern deep learning architectures.

4.1 NORMALIZATION DESIGN VIA IB PRINCIPLE

Normalization decomposition and limitations. Consider a data space \mathcal{X} and label space \mathcal{Y} with a fixed joint distribution $\mathbb{P}(X,Y) \in \mathcal{P}(\mathcal{X} \times \mathcal{Y})$. A feedforward neural network $f(\cdot;\theta)$, parameterized by θ , maps an input $X \in \mathcal{X}$ to a prediction $\hat{Y} = f(X;\theta)$, aiming to approximate the ground-truth label Y. Here, $f(\cdot;\theta)$ can represent various architectures, such as convolutional neural networks (e.g., ResNet (He et al., 2016a)) and transformer-based networks (e.g., large language models like (Touvron et al., 2023b) or vision transformer (Dosovitskiy et al., 2020)).

For an L-layer network equipped with normalization, we write the intermediate representation after the l-th normalization as

$$T_l := \Phi_l \circ h_l \circ \dots \circ \Phi_1 \circ h_1(X) \in \mathcal{T}_l, \quad l \in \{1, \dots, L\}, \tag{3}$$

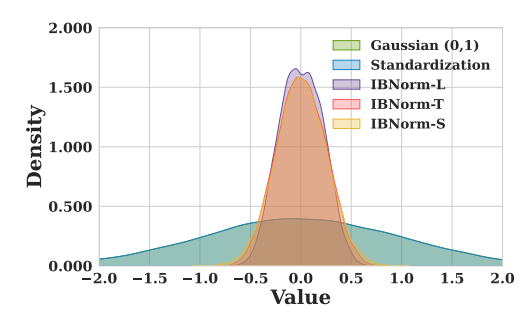
where \mathcal{T}_l is a measurable space, h_i is a transformation block with parameter θ_i , and Φ_i is the normalization layer, e.g., layer normalization. We use symbol \circ to represent the composition of functions. Following (Huang et al., 2023), any normalization layer Φ can be decomposed into three steps:

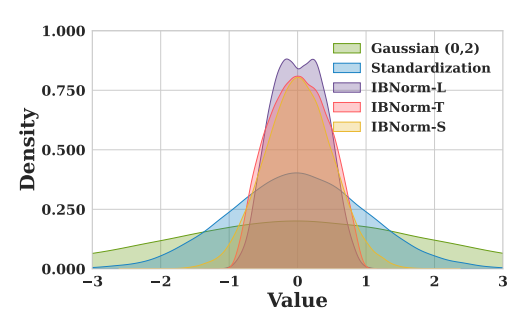
$$\Phi(\cdot) \equiv \eta \circ \psi \circ \zeta,\tag{4}$$

where ζ defines the *normalization area partitioning* (NAP), i.e., how features are grouped (e.g., batch-level in BN, feature-level in LN, or group-level in GN); ψ is the *normalization operation* (NOP), i.e., the standardization operation; η is the *normalization representation recovery* (NRR), typically an affine re-scaling and shifting.

This decomposition unifies existing normalization methods. For instance, BN (Ioffe & Szegedy, 2015), LN (Ba et al., 2016), and GN (Wu & He, 2018) differ mainly in their choice of NAP (ζ): BN normalizes across the batch dimension, LN across the feature dimension, and GN across groups of features. In all cases, the NOP enforces zero-mean and unit-variance statistics, while the NRR rescales and shifts the result. Crucially, among them, NAP (ζ) is often dictated by the network architecture or task domain (e.g., batch-based normalization favored by CNNs, feature-based normalization for Transformers). Likewise, NRR (η) is linear and invertible, and therefore only reparameterizes activations without altering their information content. This leaves the NOP (ψ) as the main degree of freedom: it governs how information is filtered and thus determines whether normalization merely stabilizes optimization or also enhances the quality of learned representations.

However, most existing NOP (ψ) operations are fundamentally variance-centric, enforcing zero-mean and unit-variance scaling of activations. While stabilizing and accelerating training, it over-looks whether the resulting representations retain task-relevant information. From the IB perspective in Sec. 3, it reveals a fundamental limitation: variance normalization alone cannot guarantee the balance between sufficiency (retaining predictive information) and minimality (removing redundancy).





(a) Under Gaussian (0,1) input.

(b) Gaussian (0,2) input.

Figure 1: Comparison of kernel density estimation for Gaussian inputs (mean 0, varying variance) under different compression operations: Standardization, IBNorm-L, IBNorm-T, and IBNorm-S ($\lambda=4$). Compression operations in IBNorm compress the tail of activations while adjusting higher-order statistics. IBNorm-L, IBNorm-T, and IBNorm-S, with the same λ , exhibit different abilities to compress the tails of activations. See more examples in Appendix C.3.

As a result, relying solely on variance-centric NOP (ψ) can produce representations with superior generalization and robustness, since higher IB values are empirically and theoretically linked to better generalization and robustness (Kawaguchi et al., 2023; Alemi et al., 2016; Goldfeld & Polyanskiy, 2020; Saxe et al., 2019; Achille & Soatto, 2018).

IB-guided normalization objective. The IB framework provides a principled way to rethink normalization. An ideal intermediate representation T_l should satisfy two criteria: 1) preserve sufficiency, namely, maximizing the predictive information $I(Y;T_l)$ about the target and thus representation T_l can easily predict the target Y; and 2) promote compression, i.e., minimizing task-nuisance information $I(T_{l-1};T_l)$ carried over from the previous layer and thereby removing the potential unimportant noises or patterns. This intuition leads to the following multi-layer IB objective:

$$\max_{\{T_l\}_{l=1}^L} \sum_{l=1}^L \Big(I(Y; T_l) - \beta I(T_{l-1}; T_l) \Big), \tag{5}$$

where $\{T_l\}_{l=1}^L \in \mathcal{T}_1 \times \cdots \times \mathcal{T}_L \equiv \mathcal{T}^{\otimes L}$, $T_0 = X$ and $\beta > 0$ controls the trade-off between sufficiency and compression. Prior works (Kawaguchi et al., 2023; Saxe et al., 2019; Alemi et al., 2016; Goldfeld & Polyanskiy, 2020; Achille & Soatto, 2018) has shown that both generalization error and robustness positively correlate with the IB value in Eqn. (5), implying that aligning intermediate representations with the IB principle can improve generalization and robustness.

Building on this insight, we aim to enhance conventional variance-centric NOP (ψ) operator with an IB-inspired compression operation. Rather than treating normalization as a mere stabilizer, we reinterpret it as an information filter that produces representations that are both compact and predictive, bridging optimization stability and information-theoretic optimality. Directly optimizing Eqn.(5) is infeasible due to costly mutual information estimation over the unknown joint distribution $p_{X,Y}$, but it provides a guiding principle: normalization should go beyond variance standardization to encourage information-preserving activations. We introduce our IB-inspired normalization in Sec.4.2 and theoretically justify its superiority and improved generalization in Sec. 4.3.

4.2 IB-INSPIRED NORMALIZATION

In the previous subsection, we identified a key limitation of existing normalization methods: their variance-centric design does not guarantee that intermediate representations preserve task-relevant information. Guided by the IB principle, our goal is to design a normalization operator that explicitly reshapes activations into information-preserving forms, rather than merely controlling their variance.

To this end, we propose an IB-inspired normalization. Unlike conventional variance-centric approaches, which manipulate only first- and second-order activation statistics via standardizing activations to have zero mean and unit variance, our approach introduces an extra compression operation into the normalization operation (NOP) ψ that acts on higher-order statistics. Specifically, ψ com-

presses activations toward their mean in a controlled manner, thereby increasing local kurtosis and inducing sparsity in activations across instances. Prior work has shown that mean-centered and sparse representations, where most activations concentrate around the mean, often exhibit stronger generalization since redundant and task-unrelated information are removed (Olshausen & Field, 1997; Ranzato et al., 2007; Bengio et al., 2013; Zhang et al., 2018; Guo et al., 2019). Motivated by this insight, our compression operation suppresses variability in activation tails, reshaping the higher-order distribution of activations rather than merely rescaling and shifting activations. More importantly, we find this design aligns normalization with the IB principle, preserving target-relevant information $I(Y; T_l)$ while suppressing irrelevant task-nuisance information $I(T_{l-1}; T_l)$.

Compression operation in IBNorm. Here we introduce the normalization operation (NOP) ψ in our IBNorm. Let X be hidden activations from a given layer, and let $\mathbf{x} = \{x_i\}_{i=1}^H$ represent a sample of H-dimensional activations. We define the compression operation $s_{\lambda}(\cdot; \lambda) : \mathbb{R}^d \to \mathbb{R}^d$ as

$$s_{\lambda}(x_i; \lambda) = \mu + \operatorname{sign}(x_i - \mu) \cdot f_{\lambda}(|x_i - \mu|), \tag{6}$$

where $\mu = \frac{1}{H} \sum_{i=1}^{H} x_i$ is the mean activation, and $f_{\lambda}(|x_i - \mu|)$ is a measurable and strictly monotone non-decreasing function with a hyper-parameter λ satisfying the *bounded compression property*:

$$0 \le f_{\lambda}(r) \le \alpha_{\lambda} r, \quad \forall r \ge 0, \quad \alpha_{\lambda} \in [0, 1].$$
 (7)

The property (7) reduces the spread of the activation distribution and increases local kurtosis and sparsity in activations by pushing more activations toward the mean. This sparsity effectively suppresses variability in the tail regions, which often encode task-irrelevant fluctuations in the high-dimensional activations (Olshausen & Field, 1997; Hyvärinen & Oja, 2000). As a result, the compression operation decreases task-nuisance information with the input, $I(T_{l-1};T_l)$, while preserving the main mass of the distribution that carries task-relevant information, $I(Y;T_l)$. In other words, by promoting sparse and mean-centered activations, compression encourages representations that retain task relevant information for the downstream task while attenuating task-nuisance information, consistent with the IB principle, which is also empirically validated in Sec. 4.3.

We instantiate three representative forms of the compression function f_{λ} : IBNorm-S, IBNorm-L, and IBNorm-T. These functionals yield different compression behaviors:

$$f_{\lambda}(|x_i - \mu|) = |x_i - \mu|/\lambda,$$
 (IBNorm-S, linear compression) (8)

$$f_{\lambda}(|x_i - \mu|) = \ln(1 + |x_i - \mu|/\lambda),$$
 (IBNorm-L, logarithmic compression) (9)

$$f_{\lambda}(|x_i - \mu|) = \tanh(|x_i - \mu|/\lambda)$$
. (**IBNorm-T**, hyperbolic tangent compression) (10)

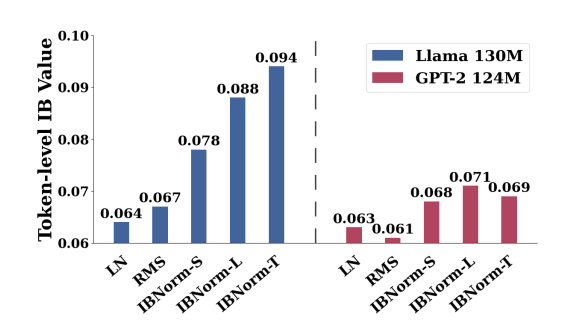
For these functionals, the compression ratio α_{λ} in Eqn. (7) becomes $\alpha_{\lambda}=1/\lambda$, guaranteeing the bounded compression property whenever $\lambda \geq 1$. So λ controls the compression strength: larger λ enforces stronger compression toward the mean μ , whereas smaller λ lead to broader activations. By suppressing the tails of the activation distribution, this reduces task-nuisance information while preserving task-relevant information. See more rationale about compression operation in Appendix C.3.

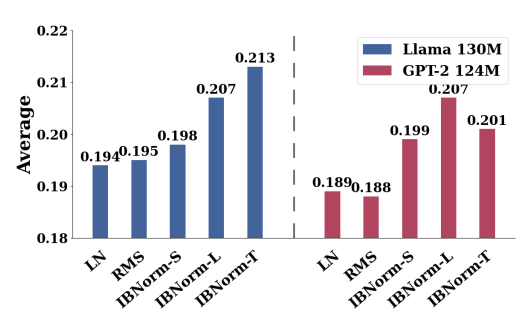
IBNorm. Building on the foundation of LayerNorm, we introduce *IBNorm*, which integrates an explicit compression operation into the normalization pipeline. This design preserves the well-known benefits of LayerNorm—training stability and acceleration and architectural compatibility—while also incorporating the information-theoretic advantages of the IB principle. Finally, we derive three varaints: IBNorm-S, IBNorm-L, and IBNorm-T.

Formally, given an activation input x, IBNorm applies the following sequence of operations: first, the NAP operator ζ partitions features in the same way as LayerNorm; next, a compression operator s_{λ} reduces nuisance variability; then, the NOP operator ψ standardizes activations; and finally, the NRR operator η rescales and shifts them:

$$IBNorm(x; \lambda) \equiv \eta \circ \psi \circ s_{\lambda} \circ \zeta. \tag{11}$$

This hybrid procedure, summarized in Algorithm 1 of Appendix A, yields a normalization strategy explicitly guided by the IB principle. By construction, IBNorm goes beyond variance normalization: it acts as an *information filter*, enhancing sufficiency by retaining predictive information while improving minimality through compression of irrelevant information in the input. In this way, IBNorm bridges the gap between practical optimization benefits and information-theoretic optimality.





- (a) Token-level IB values of Llama-130M and GPT-2 small trained on C4 and OpenWebText, respectively.
- (b) Test performance of Llama-130M and GPT-2 small evaluated on the LLM Leaderboard II.

Figure 2: Evaluation of different normalization methods on Llama-130M and GPT-2 small. (a) shows token-level IB values evaluated at the test dataset when training only the normalization layers, and (b) reports test performance on the LLM Leaderboard II.

4.3 THEORETICAL JUSTIFICATION OF IBNORM

Here we first show that IBNorm achieves a larger IB value in Eqn. (5) than standard normalization methods, and then prove its superior generalization performance.

Information-theoretic superiority of IBNorm. To analyze the impact of normalization, we consider a simplified setting with two one-layer neural networks, $f_{\rm S} = \Phi_{\rm s} \circ h$ and $f_{\rm IB} = \Phi_{\rm IB} \circ h$, that share the same feature extractor h but differ in their normalization layers: $\Phi_{\rm s} \equiv \eta \circ \psi \circ \zeta$ in the baseline network $f_{\rm s}$ and $\Phi_{IB} \equiv \eta \circ \psi \circ s_{\lambda} \circ \zeta$ in the network $f_{\rm IB}$ with IBNorm.

Given the sample dataset $S=\{x_i,y_i\}_{i=1}^M\sim \mathbb{P}(X,Y)$ containing M samples, we define the empirical IB value as $\widehat{\mathrm{IB}}_{\mathrm{S}}(T_1):=\widehat{I}_{\mathrm{S}}(Y;T_1)-\beta\widehat{I}_{\mathrm{S}}(X;T_1)$ based on Eqn. (5). Because η is linear and invertible, it does not affect the mutual information terms; therefore, it suffices to analyze the IB value of intermediate features $\widetilde{T}_s:=\psi\circ\zeta\circ h(X)$ and $\widetilde{T}_{IB}:=\psi\circ s_\lambda\circ\zeta\circ h(X)$. Based on the bounded compression property of IBNorm, we can establish the following relationship.

Theorem 1. [IB Value] For any hyperparameter $\beta \in [0,1]$ and the sample dataset $S \sim \mathbb{P}(X,Y)$ of size M, we have

 $\widehat{IB}_S(\widetilde{T}_{IB}) > \widehat{IB}_S(\widetilde{T}_s)$ almost surely.

The proof is provided in Appendix E.1. Theorem 1 establishes the theoretical advantage of IBNorm: its compressed features yield higher IB values than those from normalization with standardization, such as LN and BN. Intuitively, IBNorm better preserves label-relevant information $I(Y; \tilde{T}_{IB})$ while suppressing task-nuisance information $I(X; \tilde{T}_{IB})$, leading to more efficient and predictive representations. Crucially, this benefit holds uniformly across all trade-off parameters $\beta>0$, underscoring the robustness of IBNorm in balancing compression and informativeness.

This result aligns with our empirical observation. We train Llama-130M (Touvron et al., 2023b) and GPT-2 small (Radford et al., 2019) with frozen parameters except the normalization layers on C4 (Raffel et al., 2020) and OpenWebText (Gokaslan & Cohen, 2019), respectively. As shown in Fig. 2a, IBNorm consistently achieves higher token-level IB values ($\beta = 1$) compared to variance-centric normalizations, confirming that the compression operation directly improves information-theoretic optimality. See details in token-level IB value calculation in Appendix G.

Generalization superiority of IBNorm. We next extend the analysis to deep multi-layer networks. Based on the one-layer case, we expect IBNorm to increase IB values layer by layer, thereby enhancing both expressiveness and compression throughout the hierarchy. To formalize this, we study the generalization gap which measures difference between the expected and empirical-training loss:

$$gen(S) := \mathbb{E}_{X,Y}[\mathcal{L}(f(X),Y)] - \frac{1}{M} \sum_{i=1}^{M} \mathcal{L}(f(x_i),y_i),$$
 (12)

where \mathcal{L} denotes a per-sample loss. As shown in prior works (Zhang et al., 2016; Neyshabur et al., 2017; Hoffer et al., 2017; Jakubovitz et al., 2019), a smaller gen(S) indicates improved generalization performance and robustness both empirically and theoretically.

Table 1: Results of Llama models evaluated on LLM Leaderboard II and I. Due to space limitation,
we defer the results of each task on Leadboard I to Tab. 6 of Appendix C.1.

		I			Leaderbo	ard II			Leaderboard I
Model	Normalization	IFEval	BBH	MATH	GPQA	MUSR	MMLU-PRO	AVG	AVG
	LayerNorm	0.1479	0.2970	0.0000	0.2576	0.3426	0.1071	0.1920	0.2912
M09	RMSNorm	0.1274	0.2951	0.0000	0.2634	0.3585	0.1117	0.1924	0.2894
9	NormalNorm	0.1101	0.2876	0.0000	0.2676	0.3571	0.1166	0.1898	0.2825
Llama	IBNorm-S	0.1915	0.2732	0.0000	0.2534	0.3651	0.1152	0.1997	0.2950
i	IBNorm-L	0.1899	0.3001	0.0000	0.2772	0.3519	0.1137	0.2055	0.2955
, ,	IBNorm-T	0.1754	0.3013	0.0008	0.2668	0.3598	0.1110	0.2025	0.2937
	LayerNorm	0.1507	0.2949	0.0000	0.2650	0.3417	0.1116	0.1940	0.2921
130	RMSNorm	0.1274	0.3052	0.0008	0.2643	0.3572	0.1121	0.1945	0.2911
	NormalNorm	0.1385	0.2888	0.0000	0.2584	0.3611	0.1098	0.1928	0.2925
Llama	IBNorm-S	0.1343	0.3114	0.0008	0.2601	0.3690	0.1151	0.1984	0.2933
i	IBNorm-L	0.1836	0.3028	0.0000	0.2816	0.3638	0.1124	0.2074	0.2962
	IBNorm-T	0.1999	0.3053	0.0000	0.2777	0.3783	0.1165	0.2130	0.2970
	LayerNorm	0.1668	0.2927	0.0000	0.2659	0.3586	0.1178	0.2003	0.3062
350M	RMSNorm	0.1673	0.2999	0.0030	0.2667	0.3571	0.1121	0.2010	0.3025
	NormalNorm	0.1667	0.2940	0.0008	0.2458	0.3599	0.1103	0.1962	0.3035
Llama	IBNorm-S	0.1447	0.3020	0.0030	0.2940	0.3585	0.1094	0.2019	0.3089
اعر	IBNorm-L	0.1872	0.3135	0.0000	0.2968	0.3558	0.1162	0.2116	0.3101
-	IBNorm-T	0.1797	0.3115	0.0008	0.2983	0.3788	0.1150	0.2140	0.3089
	LayerNorm	0.1701	0.3024	0.0038	0.2691	0.3683	0.1183	0.2053	0.3138
11B	RMSNorm	0.1693	0.3005	0.0008	0.2685	0.3585	0.1139	0.2019	0.3134
	NormalNorm	0.1679	0.2971	0.0030	0.2576	0.3656	0.1127	0.2006	0.3051
Llama	IBNorm-S	0.1572	0.3118	0.0030	0.2958	0.3597	0.1130	0.2067	0.3184
\exists	IBNorm-L	0.1875	0.3167	0.0038	0.2986	0.3717	0.1171	0.2159	0.3179
	IBNorm-T	0.1829	0.3155	0.0030	0.2994	0.3793	0.1169	0.2162	0.3199

Corollary 2 (Generalization Bound). With probability at least $1 - \delta$ over training set S of size M, the generalization error of a network f_o satisfies

$$gen(S;f_o) \leq U_o := \sum\nolimits_{l=1}^L U_l^o, \ \ \textit{with} \ \ U_l = \sqrt{\frac{I(X;\tilde{T}_l^o|Y) + C(S,f_o) + \log(\frac{2}{\delta})}{M}},$$

where \tilde{T}_l^o is the intermediate representation at layer l before normalization representation recovery η and $C(S, f_o)$ is a term depending on the network f_o and the training set S. Here f_o can be the network f_S using standard normalization like LN and BN, or our network f_{IB} with our IBNorm.

See Appendix E.5 for the proof. Corollary 2 establishes that the overall generalization gap depends on the cumulative conditional mutual information across layers. This quantity,

$$I(X;\tilde{T}_l^{\mathrm{o}}|Y) \ = \ I(X;\tilde{T}_l^{\mathrm{o}}) - I(Y;\tilde{T}_l^{\mathrm{o}}) \ = \ -\mathrm{IB}(\tilde{T}_l^{\mathrm{o}}) \quad (\beta=1),$$

measures the amount of task-irrelevant input information preserved in the representations.

By Theorem 1, IBNorm increases the IB value of the population distribution at each layer, thereby reducing $I(X; \tilde{T}_l^{\rm IB}|Y)$ compared to $I(X; \tilde{T}_l^{\rm S}|Y)$. Summing across layers, we obtain $U_{\rm IB} \leq U_{\rm S}$, which shows that the generalization bound of the IBNorm network is tighter than that of the standard network. This implies that $f_{\rm IB}$ achieves superior generalization performance compared to $f_{\rm S}$. In Fig. 2b, we follow the setting in Fig. 2a to train Llama-130M and GPT-2 small. When evaluated by LLM Leaderboard II (Fourrier et al., 2024), using IBNorm can improve generation performance on downstream tasks, consistent with the information-theoretic analysis (Kawaguchi et al., 2023).

5 EXPERIMENT

We evaluate three variants—IBNorm-S, IBNorm-L, and IBNorm-T—across LLM pretraining and vision classification, comparing against LN (Ba et al., 2016), BN (Ioffe & Szegedy, 2015), RM-SNorm (Zhang & Sennrich, 2019), and NormalNorm (Eftekhari & Papyan, 2025).

LLM pretraining. We pretrain the LLaMA series (Touvron et al., 2023b) (60M-1B) on C4 (Raffel et al., 2020), following (Lialin et al., 2023; Zhao et al., 2024), and GPT-2 Small (124M) and Medium (355M) on OpenWebText (Gokaslan & Cohen, 2019), following the Sophia setup (Liu et al., 2023) with the nanoGPT implementation (Karpathy, 2022). See details in Appendix F.1. We report performance on LLM Leaderboards I & II (Beeching et al., 2023; Fourrier et al., 2024).

Table 2: Results of GPT-2 models evaluated on LLM Leaderboard II and I. Due to space limitation, we defer the results of each task on Leadboard I to Tab. 7 of Appendix C.1.

					Leaderbo	ard II			Leaderboard I
Model	Normalization	IFEval	BBH	MATH	GPQA	MUSR	MMLU-PRO	AVG	AVG
124M	LayerNorm	0.1010	0.2809	0.0000	0.2718	0.3624	0.1158	0.1886	0.2887
74	RMSNorm	0.0966	0.2772	0.0008	0.2651	0.3730	0.1154	0.1880	0.2860
	NormalNorm	0.1499	0.2913	0.0000	0.2693	0.3690	0.1119	0.1986	0.2927
GPT-2	IBNorm-S	0.1860	0.2793	0.0000	0.2619	0.3540	0.1149	0.1994	0.2934
5	IBNorm-L	0.2207	0.2850	0.0000	0.2650	0.3558	0.1134	0.2067	0.2970
	IBNorm-T	0.1836	0.2810	0.0000	0.2697	0.3571	0.1158	0.2012	0.2952
Σ	LayerNorm	0.1128	0.2835	0.0000	0.2799	0.3661	0.1106	0.1922	0.2983
355M	RMSNorm	0.1395	0.2796	0.0000	0.2694	0.3707	0.1090	0.1947	0.2950
	NormalNorm	0.1425	0.2899	0.0000	0.2702	0.3708	0.1187	0.1987	0.2955
оТ-2	IBNorm-S	0.2069	0.2802	0.0000	0.2716	0.3692	0.1176	0.2076	0.3011
G	IBNorm-L	0.2258	0.2867	0.0000	0.2771	0.3687	0.1163	0.2124	0.3035
	IBNorm-T	0.1964	0.2824	0.0008	0.2780	0.3719	0.1183	0.2080	0.3035

Table 3: Accuracy (%) on image classification tasks. We report BatchNorm's results for CNNs (ResNet18/50) since it significantly outperforms LayerNorm on CNNs, and present LayerNorm's results on Transformers (ViT) because it performs much better than BatchNorm.

	ResNet18 on CIFAR-10		ResNet5	0 on ImageNet	ViT on ImageNet		
Normalization	Top-1	Top-5	Top-1	Top-5	Top-1	Top-5	
BatchNorm	93.65	99.85	76.15	92.86	l —	_	
LayerNorm	_	_	_	_	71.54	89.40	
RMSNorm	<u> </u>	_		_	71.03	89.15	
NormalNorm	94.01	99.86	77.29	94.04	75.25	92.23	
IBNorm-S	95.49	99.85	78.85	94.03	75.82	91.97	
IBNorm-L	95.57	99.87	79.18	94.82	76.83	92.22	
IBNorm-T	95.51	99.83	78.61	93.79	76.46	92.19	

Vision training. We train ResNet-18 on CIFAR-10 (Krizhevsky et al., 2009) and ResNet-50 and ViT on ImageNet (Deng et al., 2009), following the setup (Eftekhari & Papyan, 2025). Both top-1 and top-5 accuracies are reported. Detailed settings are provided in Appendix F.2. Extended results of ViT-S/16 and ViT-B/16 (Dosovitskiy et al., 2020) on ImageNet can be found in Appendix C.2.

5.1 MAIN RESULTS

Results on LLM. Considering the space limitation and the fact that LLM Leaderboard II benchmark can more effectively evaluate the performance and is more widely used now, we defer the results of each task in Leadboard I benchmark to Appendix C.1, and only report its task average result.

As shown in Tab. 1, IBNorm consistently outperforms variance-centric normalization methods such as LN and RMSNorm. On LLaMA-60M, IBNorm-L achieves average scores of 0.2955 (Leaderboard I) and 0.2055 (Leaderboard II), improving over LN by 1.47% and 7.03%, and over RM-SNorm by 2.11% and 6.81%. On LLaMA-350M, IBNorm-L reaches 0.3101 (Leaderboard I) and 0.2140 (Leaderboard II), *i.e.* 1.27% and 6.84% over LN, and 2.03% and 9.51% over RMSNorm. On LLaMA-1B, IBNorm-T achieves the highest scores: 0.3199 on Leaderboard I and 0.2162 on Leaderboard II. Similarly, Tab. 2 also shows that on GPT-2 (355M), IBNorm-L attains 0.3035 (Leaderboard I) and 0.2124 (Leaderboard II), yielding improvements of 2.88% and 9.95% over RMSNorm.

These results demonstrate that IBNorm enhances representation quality in large language models, yielding more predictive and generalizable representations. Further analysis of mutual information and token-level IB values in Appendix C.4 confirms that IBNorm promotes representations that retain task-relevant information while suppressing nuisances, explaining the observed empirical gains.

Results for vision classification. Tab. 3 shows that IBNorm also improves performance across vision models and datasets. On CIFAR-10, ResNet18 with IBNorm-L achieves 95.57% top-1 accuracy, surpassing BN and NormalNorm by 1.92% and 1.56%. On ImageNet, ResNet50 with IBNorm-L improves over BN and NormalNorm by 3.03% and 1.89%. For ViT, IBNorm-L yields top-1 accuracy gains of 5.29%, 5.80%, and 1.58% over LN, RMSNorm, and NormalNorm, respectively.

Table 4: Ablation study of Llama 60M with normalization using different λ evaluated on LLM Leaderboard II. We defer the results of each task on Leadboard I to Tab. 9 of Appendix C.1.

Normalization	λ	IFEval	ввн	MATH	Leaderbo GPQA	ard II MUSR	MMLU-PRO	AVG	Leaderboard I AVG
	0.5	0.1687	0.2894	0.0008	0.2592	0.3519	0.1162	0.1977	0.2898
IBNorm-S	4	0.1781	0.2977	0.0000	0.2501	0.3571	0.1091	0.1987	0.2952
	8	0.1623	0.2947	0.0008	0.2606	0.3515	0.1185	0.1981	0.2918
	0.5	0.1577	0.2968	0.0000	0.2710	0.3690	0.1162	0.2018	0.2863
IBNorm-L	4	0.1899	0.3001	0.0000	0.2772	0.3519	0.1137	0.2055	0.2955
	8	0.1364	0.2888	0.0000	0.2450	0.3452	0.1132	0.1881	0.2921
	0.5	0.1761	0.3024	0.0000	0.2492	0.3469	0.1158	0.1984	0.2881
IBNorm-T	4	0.1754	0.3013	0.0008	0.2668	0.3598	0.1110	0.2025	0.2937
	8	0.1753	0.2933	0.0000	0.2559	0.3631	0.1156	0.2005	0.2898

Table 5: Ablation study of Llama 60M evaluated on LLM Leaderboard II. Due to space limitation, we defer the results of each task on Leadboard I to Tab. 8 of Appendix C.1.

		Leaderboard II										
Normalization	IFEval	BBH	MATH	GPQA	MUSR	MMLU-PRO	AVG	AVG				
IBNorm-S* IBNorm-S**	0.1626 0.1376	0.2646 0.2946	$0.0000 \\ 0.0000$	0.2876 0.2776	0.3609 0.3460	0.1114 0.1114	0.1978 0.1945	0.2952 0.2881				
IBNorm-T* IBNorm-T**	0.1372 0.1272	0.2880 0.2980	0.0000 0.0000	0.2801 0.2701	0.3519 0.3519	0.1166 0.1166	0.1956 0.1940	0.2936 0.2831				
IBNorm-L* IBNorm-L**	0.1374 0.1374	0.2941 0.2841	0.0000 0.0000	0.2793 0.2693	0.3505 0.3505	0.1190 0.1190	0.1967 0.1934	0.2905 0.2859				

5.2 ABLATION STUDY

Effects of compression hyper-parameter λ . We analyze the effect of the hyperparameter λ in our proposed IBNorm, which controls the strength of the compression on intermediate activations. Specifically, we consider $\lambda=0.5,4,8$, corresponding to mild, moderate, and strong compression, respectively. As shown in Tab. 4, the results show that moderate compression ($\lambda=4$) achieves the best performance, striking a balance between preserving task-relevant information and suppressing irrelevant variability. For instance, IBNorm-S achieves the best scores of 0.2952 and 0.1987. We find that overly mild and strong compression lead to suboptimal performance, excessively reducing the representation diversity.

Effects of operation order and affine reparameterization. To better understand the design choices in our proposed IBNorm, we conduct ablation experiments on two critical components: the operation order and the affine reparameterization. As shown in Tab. 5, IBNorm with notation * denotes applying standardization prior to the compression transformation, namely, IBNorm(x; λ) $\equiv \eta \circ s_{\lambda} \circ \psi \circ \zeta$. This modification leads to only minor fluctuations in performance compared to the baseline: for example, the baseline achieves average scores of 0.2950 and 0.1997, while IBNorm-S* obtains 0.2952 and 0.1978 on Leaderboard I and II, respectively. This shows that we should do compression and then apply standardization for better performance. In addition, IBNorm with notation ** removes the linear affine component, which consistently results in a pronounced degradation across benchmarks. For instance, IBNorm-L achieves 0.2955 and 0.2055, whereas IBNorm-L** drops to 0.2859 and 0.1934 on Leaderboard I and II, showing the importance of affine reparameterization (η).

6 Conclusion

We revisited normalization through the lens of IB principle and proposed a principled framework for designing normalization layers. Then, we introduced **IBNorm**, a family of nonlinear transforms that compress activations toward their mean, yielding more information-rich representations. Theoretically, we showed that IBNorm achieves stronger information-theoretic optimality—attaining higher IB values and tighter generalization bounds—than variance-centric methods. Empirically, IBNorm consistently outperforms BN, LN, and RMSNorm across both vision and language domains.

Limitations. Our experiments are limited to medium-scale LLMs due to computational constraints. Extending evaluations to larger foundation models is an important direction for future work.

Declaration of LLM usage. LLMs were used solely for polishing and formatting text. All research ideas, methods, and experimental results presented are original contributions of the authors.

ETHICS STATEMENT

The large language models employed in this research may reflect biases or generate sensitive or potentially offensive content, intended solely for academic and scientific purposes. The opinions expressed within generated outputs do not represent the views of the authors. We remain committed to fostering the development of AI technologies which align with ethical standards and reflect societal values.

REPRODUCIBILITY STATEMENT

We detail our work in the Methodology section (Sec. 4) and describe implementation details in Sec. 5 and Appendix F.

REFERENCES

- Alessandro Achille and Stefano Soatto. Emergence of invariance and disentanglement in deep representations. *Journal of Machine Learning Research*, 19(50):1–34, 2018.
- Alexander A Alemi, Ian Fischer, Joshua V Dillon, and Kevin Murphy. Deep variational information bottleneck. *arXiv preprint arXiv:1612.00410*, 2016.
- Jimmy Lei Ba, Jamie Ryan Kiros, and Geoffrey E Hinton. Layer normalization. *arXiv preprint* arXiv:1607.06450, 2016.
- Jinze Bai, Shuai Bai, Yunfei Chu, Zeyu Cui, Kai Dang, Xiaodong Deng, Yang Fan, Wenbin Ge, Yu Han, Fei Huang, et al. Qwen technical report. *arXiv preprint arXiv:2309.16609*, 2023.
- Edward Beeching, Clémentine Fourrier, Nathan Habib, Sheon Han, Nathan Lambert, Nazneen Rajani, Omar Sanseviero, Lewis Tunstall, and Thomas Wolf. Open Ilm leaderboard. https://huggingface.co/spaces/open-llm-leaderboard-old/open_llm_leaderboard, 2023.
- Yoshua Bengio, Aaron Courville, and Pascal Vincent. Representation learning: A review and new perspectives. *IEEE transactions on pattern analysis and machine intelligence*, 35(8):1798–1828, 2013.
- Ruidi Chang, Chunyuan Deng, and Hanjie Chen. The generalization ridge: Information flow in natural language generation. *arXiv preprint arXiv:2507.05387*, 2025.
- Harm De Vries, Florian Strub, Jérémie Mary, Hugo Larochelle, Olivier Pietquin, and Aaron C Courville. Modulating early visual processing by language. Advances in neural information processing systems, 30, 2017.
- Jia Deng, Wei Dong, Richard Socher, Li-Jia Li, Kai Li, and Li Fei-Fei. Imagenet: A large-scale hierarchical image database. In *2009 IEEE conference on computer vision and pattern recognition*, pp. 248–255. Ieee, 2009.
- Guillaume Desjardins, Karen Simonyan, Razvan Pascanu, et al. Natural neural networks. *Advances in neural information processing systems*, 28, 2015.
- Jacob Devlin, Ming-Wei Chang, Kenton Lee, and Kristina Toutanova. Bert: Pre-training of deep bidirectional transformers for language understanding. In *Proceedings of the 2019 conference of the North American chapter of the association for computational linguistics: human language technologies, volume 1 (long and short papers)*, pp. 4171–4186, 2019.
- Alexey Dosovitskiy, Lucas Beyer, Alexander Kolesnikov, Dirk Weissenborn, Xiaohua Zhai, Thomas Unterthiner, Mostafa Dehghani, Matthias Minderer, Georg Heigold, Sylvain Gelly, et al. An image is worth 16x16 words: Transformers for image recognition at scale. *arXiv preprint arXiv:2010.11929*, 2020.

- Abhimanyu Dubey, Abhinav Jauhri, Abhinav Pandey, Abhishek Kadian, Ahmad Al-Dahle, Aiesha Letman, Akhil Mathur, Alan Schelten, Amy Yang, Angela Fan, et al. The llama 3 herd of models. *arXiv e-prints*, pp. arXiv–2407, 2024.
- Daniel Eftekhari and Vardan Papyan. On the importance of gaussianizing representations. *arXiv* preprint arXiv:2505.00685, 2025.
- Marco Federici, Anjan Dutta, Patrick Forré, Nate Kushman, and Zeynep Akata. Learning robust representations via multi-view information bottleneck. *arXiv preprint arXiv:2002.07017*, 2020.
- Clémentine Fourrier, Nathan Habib, Alina Lozovskaya, Konrad Szafer, and Thomas Wolf. Open Ilm leaderboard v2. https://huggingface.co/spaces/open-llm-leaderboard/open llm leaderboard, 2024.
- Luis Gonzalo Sanchez Giraldo, Murali Rao, and Jose C Principe. Measures of entropy from data using infinitely divisible kernels. *IEEE Transactions on Information Theory*, 61(1):535–548, 2014.
- Aaron Gokaslan and Vanya Cohen. Openwebtext corpus. *Skylion007*, 2019. URL http://skylion007.github.io/OpenWebTextCorpus.
- Ziv Goldfeld and Yury Polyanskiy. The information bottleneck problem and its applications in machine learning. *IEEE Journal on Selected Areas in Information Theory*, 1(1):19–38, 2020.
- Wenzhong Guo, Jianwen Wang, and Shiping Wang. Deep multimodal representation learning: A survey. *Ieee Access*, 7:63373–63394, 2019.
- Kaiming He, Xiangyu Zhang, Shaoqing Ren, and Jian Sun. Identity mappings in deep residual networks. In *European conference on computer vision*, pp. 630–645. Springer, 2016a.
- Kaiming He, Xiangyu Zhang, Shaoqing Ren, and Jian Sun. Deep residual learning for image recognition. In *Proceedings of the IEEE conference on computer vision and pattern recognition*, pp. 770–778, 2016b.
- Elad Hoffer, Itay Hubara, and Daniel Soudry. Train longer, generalize better: closing the generalization gap in large batch training of neural networks. *Advances in neural information processing systems*, 30, 2017.
- Lei Huang, Dawei Yang, Bo Lang, and Jia Deng. Decorrelated batch normalization. In *Proceedings* of the IEEE Conference on Computer Vision and Pattern Recognition, pp. 791–800, 2018.
- Lei Huang, Jie Qin, Yi Zhou, Fan Zhu, Li Liu, and Ling Shao. Normalization techniques in training dnns: Methodology, analysis and application. *IEEE transactions on pattern analysis and machine intelligence*, 45(8):10173–10196, 2023.
- Aapo Hyvärinen and Erkki Oja. Independent component analysis: algorithms and applications. *Neural networks*, 13(4-5):411–430, 2000.
- Sergey Ioffe and Christian Szegedy. Batch normalization: Accelerating deep network training by reducing internal covariate shift. In *International conference on machine learning*, pp. 448–456. pmlr, 2015.
- Daniel Jakubovitz, Raja Giryes, and Miguel RD Rodrigues. Generalization error in deep learning. In *Compressed sensing and its applications: third international MATHEOn conference 2017*, pp. 153–193. Springer, 2019.
- Andrej Karpathy. nanogpt. *GitHub repository*, 2022. URL https://github.com/karpathy/nanoGPT.
- Kenji Kawaguchi, Zhun Deng, Xu Ji, and Jiaoyang Huang. How does information bottleneck help deep learning? In *International conference on machine learning*, pp. 16049–16096. PMLR, 2023.
- Taesup Kim, Inchul Song, and Yoshua Bengio. Dynamic layer normalization for adaptive neural acoustic modeling in speech recognition. *arXiv* preprint arXiv:1707.06065, 2017.

- Diederik Kinga, Jimmy Ba Adam, et al. A method for stochastic optimization. In *International conference on learning representations (ICLR)*, volume 5. California;, 2015.
- Alex Krizhevsky, Geoffrey Hinton, et al. Learning multiple layers of features from tiny images, 2009.
- Vladislav Lialin, Namrata Shivagunde, Sherin Muckatira, and Anna Rumshisky. Relora: High-rank training through low-rank updates, 2023. URL https://arxiv.org/abs/2307.05695.
- Qianli Liao, Kenji Kawaguchi, and Tomaso Poggio. Streaming normalization: Towards simpler and more biologically-plausible normalizations for online and recurrent learning. *arXiv* preprint *arXiv*:1610.06160, 2016.
- Aixin Liu, Bei Feng, Bing Xue, Bingxuan Wang, Bochao Wu, Chengda Lu, Chenggang Zhao, Chengqi Deng, Chenyu Zhang, Chong Ruan, et al. Deepseek-v3 technical report. arXiv preprint arXiv:2412.19437, 2024.
- Hong Liu, Zhiyuan Li, David Hall, Percy Liang, and Tengyu Ma. Sophia: A scalable stochastic second-order optimizer for language model pre-training. *arXiv preprint arXiv:2305.14342*, 2023.
- Zhuang Liu, Hanzi Mao, Chao-Yuan Wu, Christoph Feichtenhofer, Trevor Darrell, and Saining Xie. A convnet for the 2020s. In *Proceedings of the IEEE/CVF conference on computer vision and pattern recognition*, pp. 11976–11986, 2022.
- Ilya Loshchilov and Frank Hutter. Decoupled weight decay regularization. *arXiv preprint* arXiv:1711.05101, 2017.
- Behnam Neyshabur, Srinadh Bhojanapalli, David McAllester, and Nati Srebro. Exploring generalization in deep learning. *Advances in neural information processing systems*, 30, 2017.
- Bruno A Olshausen and David J Field. Sparse coding with an overcomplete basis set: A strategy employed by v1? *Vision research*, 37(23):3311–3325, 1997.
- Alec Radford, Jeffrey Wu, Rewon Child, David Luan, Dario Amodei, Ilya Sutskever, et al. Language models are unsupervised multitask learners. *OpenAI blog*, 1(8):9, 2019.
- Colin Raffel, Noam Shazeer, Adam Roberts, Katherine Lee, Sharan Narang, Michael Matena, Yanqi Zhou, Wei Li, and Peter J Liu. Exploring the limits of transfer learning with a unified text-to-text transformer. *Journal of machine learning research*, 21(140):1–67, 2020.
- Marc'Aurelio Ranzato, Y-Lan Boureau, Yann Cun, et al. Sparse feature learning for deep belief networks. *Advances in neural information processing systems*, 20, 2007.
- Tim Salimans and Durk P Kingma. Weight normalization: A simple reparameterization to accelerate training of deep neural networks. *Advances in neural information processing systems*, 29, 2016.
- Andrew M Saxe, Yamini Bansal, Joel Dapello, Madhu Advani, Artemy Kolchinsky, Brendan D Tracey, and David D Cox. On the information bottleneck theory of deep learning. *Journal of Statistical Mechanics: Theory and Experiment*, 2019(12):124020, 2019.
- Ohad Shamir, Sivan Sabato, and Naftali Tishby. Learning and generalization with the information bottleneck. *Theoretical Computer Science*, 411(29-30):2696–2711, 2010.
- Ravid Shwartz-Ziv and Naftali Tishby. Opening the black box of deep neural networks via information. *arXiv preprint arXiv:1703.00810*, 2017.
- Aliaksandr Siarohin, Enver Sangineto, and Nicu Sebe. Whitening and coloring batch transform for gans. *arXiv preprint arXiv:1806.00420*, 2018.
- Cecilia Summers and Michael J Dinneen. Four things everyone should know to improve batch normalization. *arXiv preprint arXiv:1906.03548*, 2019.
- Naftali Tishby and Noga Zaslavsky. Deep learning and the information bottleneck principle. In 2015 ieee information theory workshop (itw), pp. 1–5. Ieee, 2015.

- Naftali Tishby, Fernando C Pereira, and William Bialek. The information bottleneck method. *arXiv* preprint physics/0004057, 2000.
- Hugo Touvron, Thibaut Lavril, Gautier Izacard, Xavier Martinet, Marie-Anne Lachaux, Timothée Lacroix, Baptiste Rozière, Naman Goyal, Eric Hambro, Faisal Azhar, et al. Llama: Open and efficient foundation language models. *arXiv preprint arXiv:2302.13971*, 2023a.
- Hugo Touvron, Louis Martin, Kevin Stone, Peter Albert, Amjad Almahairi, Yasmine Babaei, Nikolay Bashlykov, Soumya Batra, Prajjwal Bhargava, Shruti Bhosale, et al. Llama 2: Open foundation and fine-tuned chat models. *arXiv preprint arXiv:2307.09288*, 2023b.
- Ashish Vaswani, Noam Shazeer, Niki Parmar, Jakob Uszkoreit, Llion Jones, Aidan N Gomez, Łukasz Kaiser, and Illia Polosukhin. Attention is all you need. *Advances in neural information processing systems*, 30, 2017.
- Yuxin Wu and Kaiming He. Group normalization. In *Proceedings of the European conference on computer vision (ECCV)*, pp. 3–19, 2018.
- Jingjing Xu, Xu Sun, Zhiyuan Zhang, Guangxiang Zhao, and Junyang Lin. Understanding and improving layer normalization. *Advances in neural information processing systems*, 32, 2019.
- Li Yuan, Yunpeng Chen, Tao Wang, Weihao Yu, Yujun Shi, Zi-Hang Jiang, Francis EH Tay, Jiashi Feng, and Shuicheng Yan. Tokens-to-token vit: Training vision transformers from scratch on imagenet. In *Proceedings of the IEEE/CVF international conference on computer vision*, pp. 558–567, 2021.
- Biao Zhang and Rico Sennrich. Root mean square layer normalization. *Advances in Neural Information Processing Systems*, 32, 2019.
- Chiyuan Zhang, Samy Bengio, Moritz Hardt, Benjamin Recht, and Oriol Vinyals. Understanding deep learning requires rethinking generalization. *arXiv preprint arXiv:1611.03530*, 2016.
- Daokun Zhang, Jie Yin, Xingquan Zhu, and Chengqi Zhang. Network representation learning: A survey. *IEEE transactions on Big Data*, 6(1):3–28, 2018.
- Jiawei Zhao, Zhenyu Zhang, Beidi Chen, Zhangyang Wang, Anima Anandkumar, and Yuandong Tian. Galore: Memory-efficient llm training by gradient low-rank projection. arXiv preprint arXiv:2403.03507, 2024.

IBNORM

Formally, given an activation input x, IBNorm applies the following sequence of operations: first, the NAP operator ζ partitions features in the same way as LayerNorm; next, a compression operator s_{λ} reduces nuisance variability; then, the NOP operator ψ standardizes activations; and finally, the NRR operator η rescales and shifts them:

$$IBNorm(\mathbf{x}; \lambda) \equiv \eta \circ \psi \circ s_{\lambda} \circ \zeta. \tag{13}$$

Here we summarize the IBNorm algorithmic steps in Algorithm 1. By construction, IBNorm goes beyond variance normalization: it acts as an *information filter*, enhancing sufficiency by retaining predictive information while improving minimality through compression of irrelevant information in the input. In this way, IBNorm bridges the gap between practical optimization benefits and information-theoretic optimality.

Algorithm 1 IB-inspired normalization (IBNorm)

- 1: **Input:** Activations $\boldsymbol{x} \in \mathbb{R}^{d \times m \times h \times w}$, hyperparameter λ 2: **Output:** Normalized activations $\boldsymbol{y} \in \mathbb{R}^{d \times m \times h \times w}$
- 3: Normalization area partitioning (NAP): $\hat{x} \leftarrow \zeta(x)$
- 4: Compression operation: $\tilde{\boldsymbol{x}} \leftarrow s_{\lambda}(\hat{\boldsymbol{x}})$
- 5: Normalization operation (NOP): $\bar{\boldsymbol{x}} \leftarrow \psi(\tilde{\boldsymbol{x}})$
- 6: Normalization representation recovery (NRR): $\hat{\boldsymbol{y}} \leftarrow \eta(\bar{\boldsymbol{x}})$
- 7: Reshape back: $\mathbf{y} \leftarrow \zeta^{-1}(\hat{\mathbf{y}})$

В NORMALNORM

We discuss the difference of our proposed IBNorm and NormalNorm here. We first provide the specific algorithm of NormalNorm in Algorithm 2.

Power Transform. Consider a random variable X from which a sample $x = \{x_i\}_{i=1}^H$ is obtained. The power transform $g(\cdot; \lambda)$ gaussianizes x by applying the following function for each x_i :

$$g(x_i; \lambda) = \begin{cases} \frac{(x_i+1)^{\lambda} - 1}{\lambda}, & x_i \ge 0, \ \lambda \ne 0\\ \log(x_i+1), & x_i \ge 0, \ \lambda = 0\\ -\frac{(-x_i+1)^{2-\lambda} - 1}{2-\lambda}, & x_i < 0, \ \lambda \ne 2\\ -\log(-x_i+1), & x_i < 0, \ \lambda = 2, \end{cases}$$
(14)

where λ is a transformation parameter typically estimated from the data to make the transformed values approximately normally distributed.

The key design difference lies in how NormalNorm and IBNorm shape hidden activation distributions. NormalNorm aims to maximize the entropy of hidden activations by applying a power transform after standardization. In contrast, our proposed IBNorm follows the IB principle and shapes the activation distributions via a *compression operation* applied *before* standardization.

While NormalNorm also attempts to explicitly shape activation distributions, encouraging Gaussianlike features through the power transform with additive noise, this approach has several limitations. In practice, we find that dynamically varying λ not only increases computational cost, but can also lead to training instability due to numerical issues, especially in the setting of lower precision like bfloat16. Furthermore, because the power transform modifies both the first- and second-order statistics of the hidden activations, the resulting outputs after the NOP no longer have zero mean and unit variance. As a result, the network cannot fully benefit from traditional normalization techniques, such as improved training stability and scale invariance.

Algorithm 2 Normal Normalization

Input:
$$m{u} = \{u_i\}_{i=1}^N$$

Input: $m{y} = \{y_i\}_{i=1}^N$
Learnable Parameters: γ, β

Noise Factor: $\xi \ge 0$ Standardization: Standardization: $\hat{u} \leftarrow \frac{1}{N} \sum_{i=1}^{N} u_{i}$ $\hat{\sigma}^{2} \leftarrow \frac{1}{N} \sum_{i=1}^{N} (u_{i} - \hat{u})^{2}$ $c_{i} \leftarrow \frac{u_{i} - \hat{\mu}}{\sqrt{\hat{\sigma}^{2} + \epsilon}}$ Power Transform and Scaled Additive Noise:

 $x_i \leftarrow g(c_i; \hat{\lambda})$

with gradient tracking disabled:

with gradient tracking
$$\bar{x} = \frac{1}{N} \sum_{i=1}^{N} x_i$$

$$s = \frac{1}{N} \sum_{i=1}^{N} |x_i - \bar{x}|$$
 sample $z_i \sim \mathcal{N}(0, 1)$
$$v_i = x_i + z_i \cdot s \cdot \xi$$
 Affine Transform:
$$y_i \leftarrow \gamma \cdot v_i + \beta$$

EXTENDED EMPIRICAL RESULTS

C.1 RESULTS ON LLM LEADERBOARD I

Table 6: Results of Llama models evaluated on LLM Leaderboard I.

Model	Normalization	ARC	HellaSwag	MMLU	TruthfulQA	Winogrande	GSM8K	AVG
	LayerNorm	0.2150	0.2725	0.2557	0.4935	0.5075	0.0031	0.2912
	RMSNorm	0.2244	0.2783	0.2496	0.4761	0.5059	0.0023	0.2894
Llomo 60M	NormalNorm	0.2270	0.2504	0.2295	0.4925	0.4957	0.0000	0.2825
Llama 60M	IBNorm-S	0.2631	0.2616	0.2526	0.4899	0.5028	0.0000	0.2950
	IBNorm-L	0.2568	0.2651	0.2689	0.4966	0.4854	0.0000	0.2955
	IBNorm-T	0.2270	0.2758	0.2620	0.4827	0.5099	0.0049	0.2937
	LayerNorm	0.2312	0.2795	0.2562	0.4754	0.5059	0.0042	0.2921
	RMSNorm	0.2210	0.2950	0.2494	0.4639	0.5154	0.0019	0.2911
Llama 130M	NormalNorm	0.2244	0.2684	0.2621	0.4797	0.5178	0.0027	0.2925
Liailia 130ivi	IBNorm-S	0.2295	0.2950	0.2616	0.4698	0.5012	0.0027	0.2933
	IBNorm-L	0.2577	0.2697	0.2697	0.4892	0.4891	0.0019	0.2962
	IBNorm-T	0.2267	0.2900	0.2619	0.4949	0.5043	0.0042	0.2970
	LayerNorm	0.2355	0.3286	0.2579	0.4889	0.5225	0.0038	0.3062
	RMSNorm	0.2432	0.3155	0.2513	0.5201	0.4808	0.0038	0.3025
Llama 350M	NormalNorm	0.2398	0.3031	0.2618	0.4998	0.5107	0.0057	0.3035
Liailia 330ivi	IBNorm-S	0.2363	0.3463	0.2620	0.4917	0.5149	0.0023	0.3089
	IBNorm-L	0.2619	0.3342	0.2692	0.4966	0.4949	0.0038	0.3101
	IBNorm-T	0.2598	0.3346	0.2623	0.4957	0.4970	0.0038	0.3089
	LayerNorm	0.2364	0.3711	0.2580	0.4882	0.5226	0.0064	0.3138
	RMSNorm	0.2517	0.3593	0.2522	0.5035	0.5093	0.0045	0.3134
Llama 1B	NormalNorm	0.2244	0.3183	0.2713	0.4961	0.5170	0.0038	0.3051
Liailia 1B	IBNorm-S	0.2551	0.3749	0.2636	0.4923	0.5188	0.0057	0.3184
	IBNorm-L	0.2632	0.3725	0.2691	0.4945	0.4980	0.0099	0.3179
	IBNorm-T	0.2654	0.3809	0.2663	0.4952	0.5075	0.0042	0.3199

Table 7: Results of GPT-2 models evaluated on LLM Leaderboard I.

Model	Normalization	ARC	HellaSwag	MMLU	TruthfulQA	Winogrande	GSM8K	AVG
	LayerNorm	0.2483	0.2667	0.2371	0.4868	0.4933	0.0000	0.2887
	RMSNorm	0.2551	0.2540	0.2373	0.4848	0.4838	0.0008	0.2860
GPT-2 124M	NormalNorm	0.2645	0.0000	0.2632	0.2457	0.4890	0.4941	0.2927
	IBNorm-S	0.2690	0.2558	0.2458	0.4846	0.5053	0.0000	0.2934
	IBNorm-L	0.2756	0.2577	0.2689	0.4859	0.4933	0.0008	0.2970
	IBNorm-T	0.2734	0.2569	0.2394	0.4835	0.5178	0.0004	0.2952
	LayerNorm	0.2637	0.2772	0.2485	0.4945	0.5051	0.0011	0.2983
	RMSNorm	0.2643	0.2673	0.2518	0.4951	0.4917	0.0000	0.2950
GPT-2 355M	NormalNorm	0.2601	0.2683	0.2549	0.4948	0.4949	0.0000	0.2955
	IBNorm-S	0.2781	0.2679	0.2581	0.4955	0.5072	0.0000	0.3011
	IBNorm-L	0.2813	0.2681	0.2693	0.4964	0.5058	0.0000	0.3035
	IBNorm-T	0.2819	0.2693	0.2532	0.4972	0.5185	0.0011	0.3035

Table 8: Ablation study of Llama 60M evaluated on LLM Leaderboard I.

Normalization	ARC	HellaSwag	MMLU	TruthfulQA	Winogrande	GSM8K AVG
IBNorm-S* IBNorm-S**	0.2661	0.2698	0.2542	0.4788	0.5012	0.0011 0.2952
	0.2587	0.2570	0.2535	0.4750	0.4822	0.0023 0.288
IBNorm-T* IBNorm-T**	0.2518	0.2658	0.2570	0.4879	0.4988	0.0004 0.2930
	0.2261	0.2562	0.2472	0.4740	0.4941	0.0008 0.283
IBNorm-L* IBNorm-L**	0.2483	0.2615	0.2389	0.5029	0.4886	0.0030 0.2903
	0.2435	0.2606	0.2407	0.4743	0.4957	0.0008 0.2859

Table 9: Ablation study of Llama 60M with normalization using different λ evaluated on LLM Leaderboard I.

Normalization	Normalization λ		HellaSwag	MMLU	TruthfulQA	Winogrande	GSM8K A	VG
	0.5	0.2227	0.2641	0.2478	0.4948	0.5046	0.0045 0.2	2898
IBNorm-S	4	0.2393	0.2665	0.2496	0.5033	0.5078	0.0049 0.2	2952
	8	0.2270	0.2647	0.2579	0.4984	0.4958	0.0072 0.2	2918
	0.5	0.2193	0.2781	0.2501	0.4892	0.4767	0.0045 0.2	2863
IBNorm-L	4	0.2568	0.2651	0.2689	0.4966	0.4854	0.0000 0.2	2955
	8	0.2722	0.2692	0.2293	0.4853	0.4964	0.0000 0.2	2921
	0.5	0.2243	0.2644	0.2692	0.4846	0.4862	0.0000 0.2	2881
IBNorm-T	4	0.2270	0.2758	0.2620	0.4827	0.5099	0.0049 0.2	2937
	8	0.2274	0.2645	0.2519	0.4923	0.5028	0.0000 0.2	2898

C.2 RESULTS ON IMAGENET

In addition to the results for ViT in Tab. 3, we conduct ViT experiments following the ViT-S/16 and ViT-B/16 settings (Yuan et al., 2021), with details provided in Appendix F.2.

Table 10: Accuracy (%) of ViT-S/16 and ViT-B/16 on image classification tasks. We present Layer-Norm's results on Vision Transformer (ViT) because it performs much better than BatchNorm.

	ViT-S/16	on ImageNet	ViT-B/16 on ImageNet		
Normalization	Top-1	Top-5	Top-1	Top-5	
BatchNorm	<u> </u>	_	<u> </u>	_	
LayerNorm	78.25	94.12	81.09	95.57	
RMSNorm	78.19	93.98	81.06	95.50	
NormalNorm	78.77	94.21	81.03	95.46	
IBNorm-S	80.23	94.94	82.53	95.97	
IBNorm-L	80.57	95.12	83.69	96.43	
IBNorm-T	80.76	95.21	83.71	96.49	

C.3 THE EFFECT OF COMPRESSION OPERATION IN IBNORM

We instantiate three representative forms of the compression function f_{λ} : linear (IBNorm-S), logarithmic (IBNorm-L), and hyperbolic tangent (IBNorm-T).

$$f_{\lambda}(|x_i - \mu|) = |x_i - \mu|/\lambda,$$
 (IBNorm-S, linear compression)
 $f_{\lambda}(|x_i - \mu|) = \ln(1 + |x_i - \mu|/\lambda),$ (IBNorm-L, logarithmic compression)

$$f_{\lambda}(|x_i - \mu|) = \tanh(|x_i - \mu|/\lambda)$$
. (**IBNorm-T**, hyperbolic tangent compression)

These choices capture complementary compression behaviors. Specifically, IB-S provides a linear baseline, IB-L yields progressively stronger suppression of large activations, and IB-T enforces a hard saturation effect on extreme values. Together, they span the spectrum from mild to strong tail suppression while sharing the desirable properties of boundedness and monotonicity. While other monotonic compression functions are possible, we provide these three forms to demonstrate the range of behaviors and provide a principled comparison.

The bounded compression property requires

$$0 \le f_{\lambda}(r) \le \alpha_{\lambda} r, \quad \forall r \ge 0, \quad \alpha_{\lambda} \in [0, 1].$$

To determine α_{λ} , we analyze the ratio $f_{\lambda}(r)/r$.

Linear. For $f_{\lambda}(r) = r/\lambda$,

$$\frac{f_{\lambda}(r)}{r} = \frac{1}{\lambda}, \quad \forall r > 0,$$

thus $\alpha_{\lambda} = 1/\lambda$.

Logarithmic. For $f_{\lambda}(r) = \log(1 + r/\lambda)$,

$$\frac{f_{\lambda}(r)}{r} = \frac{\log(1 + r/\lambda)}{r},$$

which is monotonically decreasing in r and attains its maximum at $r \to 0$:

$$\lim_{r \to 0} \frac{\log(1 + r/\lambda)}{r} = \frac{1}{\lambda}.$$

Hence $\alpha_{\lambda} = 1/\lambda$.

Hyperbolic tangent. For $f_{\lambda}(r) = \tanh(r/\lambda)$, the ratio

$$\frac{f_{\lambda}(r)}{r}$$

is maximized as $r \to 0$, giving

$$\lim_{r \to 0} \frac{\tanh(r/\lambda)}{r} = \frac{1}{\lambda}.$$

Thus $\alpha_{\lambda} = 1/\lambda$.

In conclusion, for these functionals, the compression ratio α_{λ} in Eqn. (7) is given by $\alpha_{\lambda} = 1/\lambda$, which guarantees the bounded compression property whenever $\lambda \geq 1$.

Compression operations in IBNorm compress the tail of activations while adjusting higher-order statistics. IBNorm-L, IBNorm-T, and IBNorm-S exhibit different abilities to compress the tails of activations.

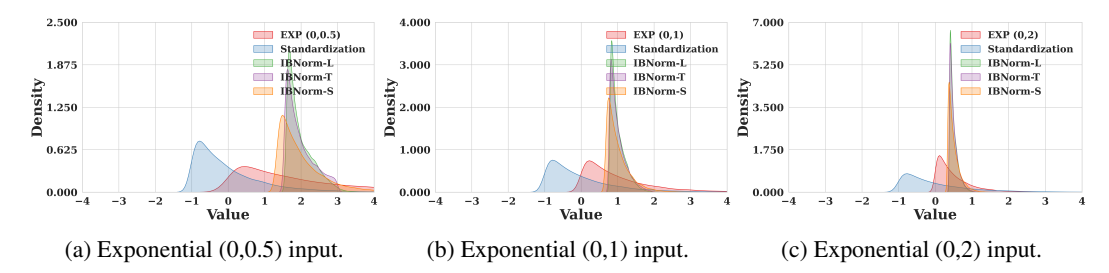


Figure 3: Comparison of kernel density estimation across different compression operation (Standardization, IBNorm-L ($\lambda=4$), IBNorm-T ($\lambda=4$), IBNorm-S ($\lambda=3$)) given Exponential distribution inputs with mean 0 and different lambdas. Compression operations in IBNorm compress the tail in the activations and adjust the higher-order statistics.

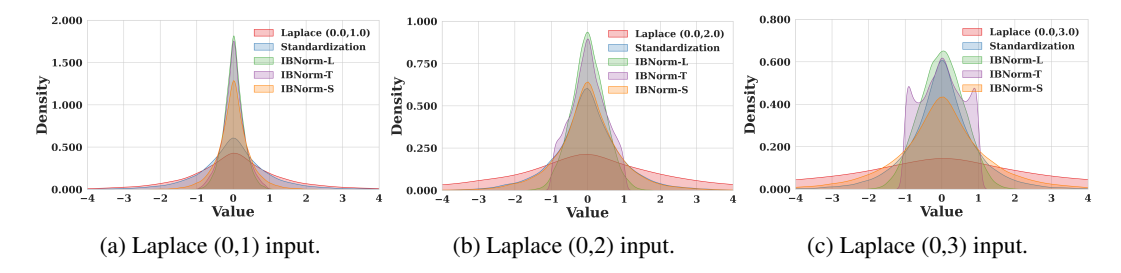


Figure 4: Comparison of kernel density estimation across different compression operation (Standardization, IBNorm-L ($\lambda=4$), IBNorm-T ($\lambda=4$), IBNorm-S ($\lambda=3$)) given Laplace distribution inputs with mean 0 and different scales. Compression operations in IBNorm compress the tail in the activations and adjust the higher-order statistics.

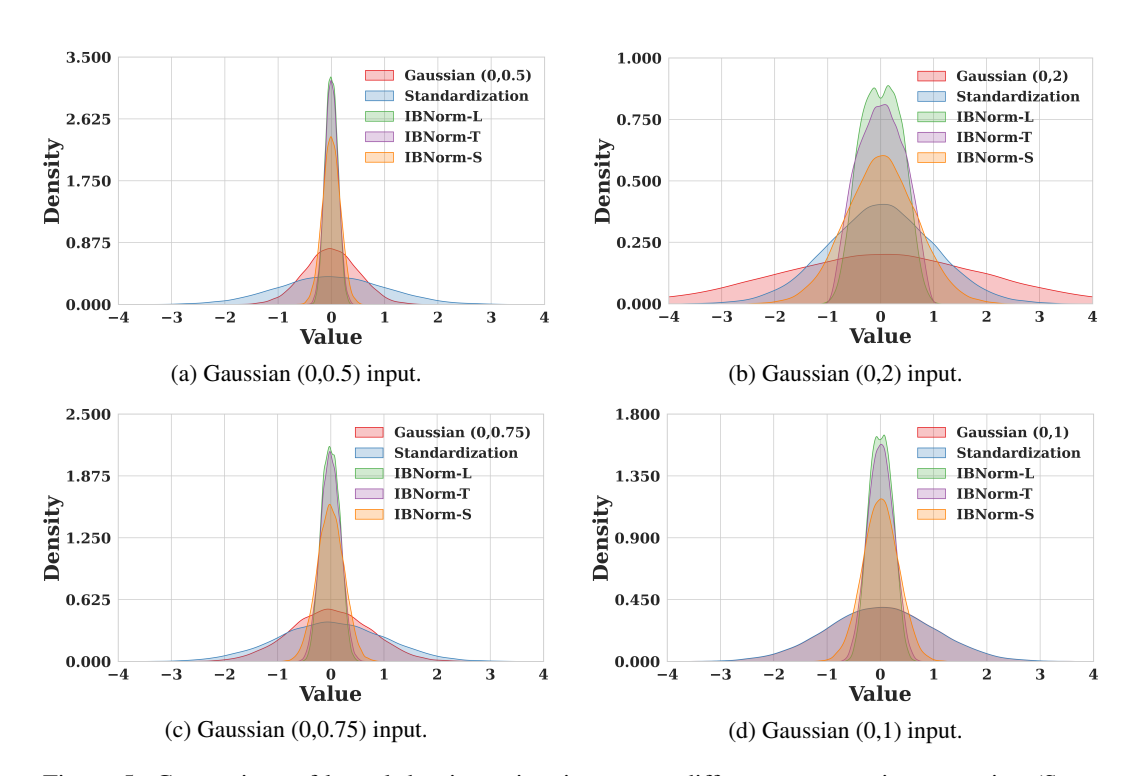


Figure 5: Comparison of kernel density estimation across different compression operation (Standardization, IBNorm-L ($\lambda=4$), IBNorm-T ($\lambda=4$), IBNorm-S ($\lambda=3$)) given Gaussian distribution inputs with mean 0 and different variance. Compression operations in IBNorm compress the tail in the activations and adjust the higher-order statistics.

C.4 ESTIMATED MUTUAL INFORMATION QUANTITIES AND TOKEN-LEVEL IB VALUE ACROSS TRAINING

We track the evolution of three mutual information quantities during training: predictive information $\hat{I}(Y;T_l)$, task–nuisance information $\hat{I}(T_{l-1};T_l)$, and their token-level IB value $\hat{I}(Y;T_l)-\hat{I}(T_{l-1};T_l)$. These quantities are measured throughout training on test dataset for Llama-130M and GPT-2 (124M) on C4 and OpenWebText, respectively. The details in token-level IB value calculation are in Appendix G.

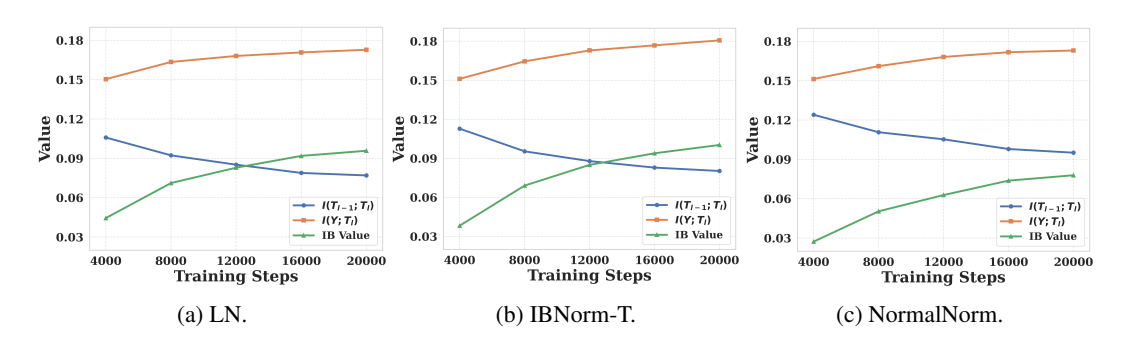


Figure 6: Evolution of predictive information $\hat{I}(Y;T_l)$, task–nuisance information $\hat{I}(T_{l-1};T_l)$, and the token-level IB value during training of Llama-130M on C4, using LN, IBNorm-T, and Normal-Norm. Results are reported on the test set.

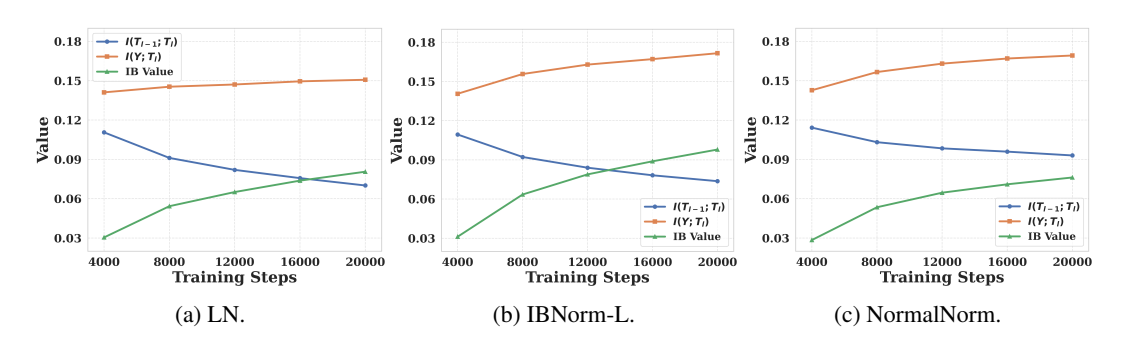


Figure 7: Evolution of predictive information $\hat{I}(Y;T_l)$, task–nuisance information $\hat{I}(T_{l-1};T_l)$, and the token-level IB value during training of GPT-2 (124M) on OpenWebText, using LN, IBNorm-L, and NormalNorm. Results are reported on the test set.

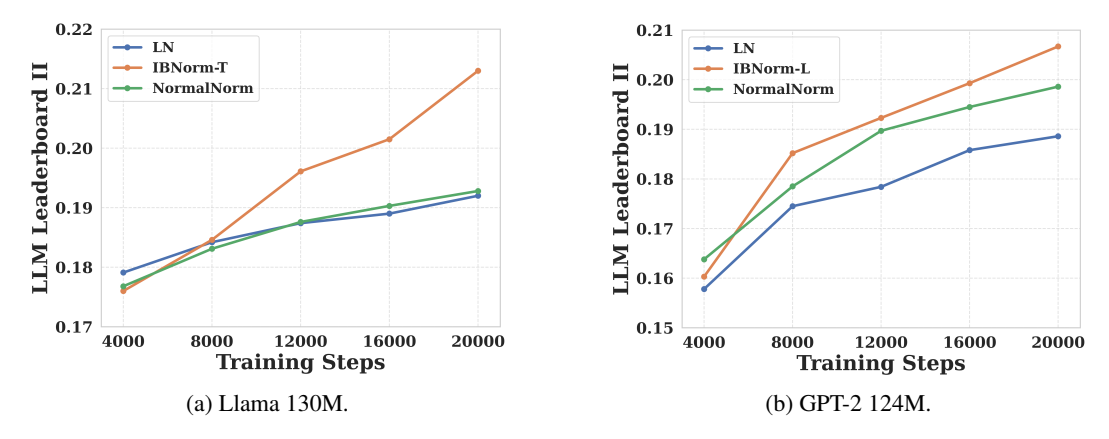


Figure 8: Evaluation of Llama 130M and GPT-2 124M trained with LN, IBNorm-L, NormalNorm on LLM Leaderboard II across training.

As shown in Figs. 6, 7, and 8, these results demonstrate that IBNorm encourages representations that retain task-relevant information while suppressing irrelevant task-nuisance information, providing a explanation for the observed empirical gains.

D DETAILS OF OTHER TERMS

We have

$$\begin{split} &G(\sigma_{H_{1}|X},\sigma_{H_{1}|Y},\sigma_{p_{1}|X},\sigma_{p_{1}|Y},\mu_{p_{1}|X},\mu_{p_{1}|Y})\\ &=C_{1}\sqrt{\frac{\sigma_{H_{1}|X}}{M}}+C_{1}\sqrt{\frac{\sigma_{H_{1}|Y}}{M}}+\sum_{y}p(y)\int_{\mathcal{T}_{1}}\phi(\sqrt{\sigma_{p_{1}|Y}})\,dt+\beta\sum_{x}p(x)\int_{\tilde{\mathcal{T}}_{1}}\phi(\sqrt{\sigma_{p_{1}|X}})\,dt\\ &+(\beta+2)\int_{\tilde{\mathcal{T}}_{1}}\phi\Big(C_{1}\sqrt{\frac{\sigma_{H_{1}|X}}{M}}\Big)p_{\tilde{T}_{1}}(t)\,dt+\sum_{y}p(y)\int_{\tilde{\mathcal{T}}_{1}}\phi(\mu_{p_{1}|Y})\,dt+\beta\sum_{x}p(x)\int_{\tilde{\mathcal{T}}_{1}}\phi(\mu_{p_{1}|X})\,dt\\ &+(\beta+1)\int_{\tilde{\mathcal{T}}_{1}}\sum_{x}p(x)[\phi(\sqrt{\sigma_{p_{1}|X}})+\phi(\mu_{p_{1}|X})]dt, \end{split}$$

where

$$\begin{split} \sigma_{H_1|X} &:= V(H(\tilde{T}_1|X)) = |\mathcal{X}| \mathbb{V}(H(\tilde{T}_1|X)), \quad \sigma_{H_1|Y} := V(H(\tilde{T}_1|Y)) = |\mathcal{Y}| \mathbb{V}(H(\tilde{T}_1|Y)), \\ \sigma_{p_1|X} &:= V(p(\tilde{T}_1|X)) = |\mathcal{X}| \mathbb{V}(p(\tilde{T}_1|X)), \qquad \sigma_{p_1|Y} := V(p(\tilde{T}_1|Y)) = |\mathcal{Y}| \mathbb{V}(p(\tilde{T}_1|Y)), \\ \mu_{p_1|X} &:= \mathbb{E}[p(\tilde{T}_1|X)], \qquad \qquad \mu_{p_1|Y} := \mathbb{E}[p(\tilde{T}_1|Y)], \end{split}$$

and

$$C_1 = 2 + \sqrt{2\log((|\mathcal{Y}| + 2)/\delta)}.$$

In addition, we have the optimum-dependent term:

$$\begin{split} Q(\tilde{T}_{1}^{*}) &= (2 + \sqrt{2 \log((|\mathcal{Y}| + 2)/\delta)}) \sqrt{\frac{V(H(\tilde{T}_{1}^{*}|Y))}{M}} \\ &+ \beta (2 + \sqrt{2 \log((|\mathcal{Y}| + 2)/\delta)}) \sqrt{\frac{V(H(\tilde{T}_{1}^{*}|X))}{M}} \\ &+ (\beta + 2) \int_{\tilde{T}_{1}^{*}} \phi \left((2 + \sqrt{2 \log((|\mathcal{Y}| + 2)/\delta)}) \sqrt{\frac{V(p(\tilde{T}_{1}^{*}|X))}{M}} \right) p_{\tilde{T}_{1}^{*}}(t) \, dt \\ &+ \sum_{y} p(y) \int_{\tilde{T}_{1}} \phi(p_{\tilde{T}_{1}^{*}|Y}(t|y)) \, dt + \beta \sum_{x} p(x) \int_{\tilde{T}_{1}} \phi(p_{\tilde{T}_{1}^{*}|X}(t|x)) \, dt + (\beta + 1) \int_{\tilde{T}_{1}} \phi(p(\tilde{T}_{1}^{*})) \, dt \\ &+ (\beta + 1) \int_{\tilde{T}_{1}} \sum_{x} p(x) \phi(p_{\tilde{T}_{1}^{*}|X}(t|x)) dt \end{split}$$

E PROOF

E.1 Proof for Theorem 1

Theorem. For any hyperparameter $\beta \in [0,1]$ and the sample set $S \sim \mathbb{P}(X,Y)$ of size M, we have

$$\widehat{\mathit{IB}}_S(\widetilde{T}_{IB}) \geq \widehat{\mathit{IB}}_S(\widetilde{T}_s)$$
 almost surely.

Proof. Given the dataset $S \sim \mathbb{P}_{X,Y}$ with size M and one-layer neural networks, $f_1 = \Phi_1 \circ h$. We analyze the IB value of intermediate features $\tilde{T}_1 := \psi \circ \zeta \circ h(X)$. First, we define the empirical gap $\Delta_S(\tilde{T}_1; \tilde{T}_1^*)$ between the IB bottleneck derived from arbitrary representation \tilde{T}_1 and the optimum representation \tilde{T}_1^* , *i.e.*

$$\Delta_{S}(\tilde{T}_{1}; \tilde{T}_{1}^{*}) = |\left(\hat{I}(Y; \tilde{T}_{1}) - \beta \hat{I}(\tilde{T}_{0}; \tilde{T}_{1})\right) - \left(\hat{I}(Y; \tilde{T}_{1}^{*}) - \beta \hat{I}(\tilde{T}_{0}^{*}; \tilde{T}_{1}^{*})\right)|, \tag{15}$$

where $\tilde{T}_0 = \tilde{T}_0^* = X$.

We prove $\widehat{\mathrm{IB}}_1 \geq \widehat{\mathrm{IB}}_2$ by showing that $\Delta_S(\widetilde{T}_{IB}; \widetilde{T}_1^*) \leq \Delta_S(\widetilde{T}_s; \widetilde{T}_1^*)$.

Lemma 3. Given a fixed trade-off hyperparameter $\beta > 0$ and a confidence parameter $\delta \in (0,1)$, the following holds with probability at least $1 - \delta$ over any sample set $S \sim \mathbb{P}(X,Y)$ with size M: for any representation $\tilde{T}_1 \in \tilde{T}_1$,

$$\Delta_S(\tilde{T}_1; \tilde{T}_1^*) \le G(\sigma_{H_1|X}, \sigma_{H_1|Y}, \sigma_{p_1|X}, \sigma_{p_1|Y}, \mu_{p_1|X}, \mu_{p_1|Y}) + Q(T_1^*). \tag{16}$$

where $G(\cdot)$ is a monotonically increasing function with its arguments. Specifically, $\sigma_{H_1|X} := \mathbb{V}(H(\tilde{T}_1|X)), \sigma_{H_1|Y} := \mathbb{V}(H(\tilde{T}_1|Y)), \sigma_{p_1|X} := \mathbb{V}(p(\tilde{T}_1|X)), \sigma_{p_1|Y} := \mathbb{V}(p(\tilde{T}_1|Y)), \mu_{p_1|X} := \mathbb{E}[p(\tilde{T}_1|X)], \mu_{p_1|Y} := \mathbb{E}[p(\tilde{T}_1|Y)]$ and \mathbb{V} is the variance function.

The formulas of concrete form of G and Q are given in Appendix D. The proof is given in Appendix E.2.

We now analyze the gap $\Delta_S(\tilde{T}_{IB}; \tilde{T}_1^*)$ and $\Delta_S(\tilde{T}_s; \tilde{T}_1^*)$ by analyzing the \tilde{T}_1 relevant terms. We first note that we have the following property for the IBNorm.

Proposition 4 (Entropy Reduction). For any random vector $Z \in \mathbb{R}^d$ with distribution \mathbb{P}_Z , the compression operation s_{λ} in IBNorm satisfies

$$H(s_{\lambda}(Z)) \le H(Z),$$
 (17)

where $H(\cdot)$ denotes differential entropy. The detailed proof is given in Appendix E.3.

Based on Proposition 4, we have the following lemma.

Lemma 5. 1) Let $\tilde{T}_{IB} = s_{\lambda}(\tilde{T}_s)$, where s_{λ} is a bounded-compression mapping with Lipschitz constant $L_1 = \prod_{i=1}^d \frac{1}{\lambda}$. For any small $\delta > 0$, the following holds:

$$\mathbb{P}(\mathbb{V}(H(\tilde{T}_{IB}|X)) \leq \mathbb{V}(H(\tilde{T}_{s}|X))) \geq 1 - \delta, \quad \mathbb{P}(\mathbb{V}(H(\tilde{T}_{IB}|Y)) \leq \mathbb{V}(H(\tilde{T}_{s}|Y))) \geq 1 - \delta.$$

2) In addition, let $\tilde{T}_1, \tilde{T}'_1 \in \tilde{\mathcal{T}}_1$ be two arbitrary elements in the representation space. Then, for any $\delta \in (0,1)$, the following holds with probability at least $1-\delta$:

$$\begin{split} &|\mathbb{V}(p(\tilde{T}_1|X)) - \mathbb{V}(p(\tilde{T}_1'|X))| \leq \delta, \\ &|\mathbb{V}(p(\tilde{T}_1|Y)) - \mathbb{V}(p(\tilde{T}_1'|Y))| \leq \delta, \\ &|\mathbb{E}[p(\tilde{T}_1|X)] - \mathbb{E}[p(\tilde{T}_1'|X)]| \leq \delta, \\ &|\mathbb{E}[p(\tilde{T}_1|Y)] - \mathbb{E}[p(\tilde{T}_1'|Y)]| \leq \delta, \end{split}$$

where the expectation and variance are taken with respect to the Lebesgue measure on $\mathcal{X} \times \mathcal{Y}$.

The detailed proof is given in Appendix E.4.

Since $G(\cdot)$ is monotone in its variance arguments, Lemma 5 implies that, for a fixed trade-off hyperparameter $\beta \in [0,1]$ and confidence parameter $\delta \in (0,1)$, with probability at least $1-\delta$ over the sample set $S \sim \mathbb{P}(X,Y)$ with size M, the following inequality holds:

$$\Delta_S(\tilde{T}_{IB}; \tilde{T}_1^*) \le \Delta_S(\tilde{T}_s; \tilde{T}_1^*).$$

Thus, given the hyperparameter β and the sample set $S \sim \mathbb{P}(X,Y)$ with size M, we have

$$\widehat{\operatorname{IB}}_S(\widetilde{T}_{IB}) \geq \widehat{\operatorname{IB}}_S(\widetilde{T}_s)$$
 almost surely.

E.2 PROOF FOR LEMMA 3

Lemma. Given a fixed trade-off hyperparameter $\beta > 0$ and a confidence parameter $\delta \in (0,1)$, the following holds with probability at least $1-\delta$ over the sample set S: for any representation $\tilde{T}_1 \in \tilde{T}_1$,

$$\Delta_{\mathcal{S}}(\tilde{T}_1; \tilde{T}_1^*) \le G(\sigma_{H_1|X}, \sigma_{H_1|Y}, \sigma_{p_1|X}, \sigma_{p_1|Y}, \mu_{p_1|X}, \mu_{p_1|Y}) + Q(T_1^*). \tag{18}$$

where $G(\cdot)$ is a monotonically increasing function with its arguments. Specifically, $\sigma_{H_1|X} := \mathbb{V}(H(\tilde{T}_1|X)), \sigma_{H_1|Y} := \mathbb{V}(H(\tilde{T}_1|Y)), \sigma_{p_1|X} := \mathbb{V}(p(\tilde{T}_1|X)), \sigma_{p_1|Y} := \mathbb{V}(p(\tilde{T}_1|Y)), \mu_{p_1|X} := \mathbb{E}[p(\tilde{T}_1|X)], \mu_{p_1|Y} := \mathbb{E}[p(\tilde{T}_1|Y)]$ and \mathbb{V} is the variance function.

The formulas of concrete form of G and Q are given in Appendix D.

Proof. Let \tilde{T}_1 be the embeddings derived from a neural network based on the sample set S.

We define the population IB value as $\mathrm{IB}(T) := I(Y;T) - \beta I(X;T)$ and empirical IB value as $\widehat{\mathrm{IB}}(T) := \widehat{I}(Y;T) - \beta \widehat{I}(X;T)$ for brevity. We denote the optimum IB representation achieving the maximum population IB value by \widetilde{T}_1^* .

We define the optimum \tilde{T}_1^* of one-layer IB objective as:

$$\tilde{T}_1^* \in \underset{\tilde{T}_1}{\operatorname{arg\,max}} (I(Y; \tilde{T}_1) - \beta I(\tilde{T}_0; \tilde{T}_1)), \tag{19}$$

where $\tilde{T}_0 = X$.

Given the dataset $S \sim \mathbb{P}_{X,Y}$ with size M, we consider the empirical gap $\Delta_{\mathbb{S}}(\tilde{T}_1; \tilde{T}_1^*)$ between the IB bottleneck derived from arbitrary representation \tilde{T}_1 and the optimum representation \tilde{T}_1^* , *i.e.*

$$\Delta_{S}(\tilde{T}_{1}; \tilde{T}_{1}^{*}) = |\left(\hat{I}(Y; \tilde{T}_{1}) - \beta \hat{I}(\tilde{T}_{0}; \tilde{T}_{1})\right) - \left(\hat{I}(Y; \tilde{T}_{1}^{*}) - \beta \hat{I}(\tilde{T}_{0}^{*}; \tilde{T}_{1}^{*})\right)|, \tag{20}$$

where $\tilde{T}_0 = \tilde{T}_0^* = X$. We have:

$$\Delta_{S}(\tilde{T}_{1}; \tilde{T}_{1}^{*}) = \left| \left(\hat{I}(Y; \tilde{T}_{1}) - \beta \hat{I}(X; \tilde{T}_{1}) \right) - \left(\hat{I}(Y; \tilde{T}_{1}^{*}) - \beta \hat{I}(X; \tilde{T}_{1}^{*}) \right) \right|$$
(21)

$$\leq \underbrace{\left| \left(\hat{I}(Y; \tilde{T}_1) - \hat{I}(Y; \tilde{T}_1^*) \right) \right|}_{I} + \underbrace{\beta \left| \left(\hat{I}(X; \tilde{T}_1) - \hat{I}(X; \tilde{T}_1^*) \right) \right|}_{II} \tag{22}$$

For any real-valued vector $\mathbf{a}=(a_1,\cdots,a_n)$, we define the function $V(\mathbf{a})=\sum_{i=1}^n(a_i-\frac{1}{n}\sum_{j=1}^na_j)^2$. Note that $\frac{1}{n}V(\mathbf{a})$ is simply the variance of the elements of \mathbf{a} .

In addition, we define an auxiliary real-valued function

$$\phi(x) = \begin{cases} -\frac{1}{e}, & x < -\frac{1}{e}, \\ -x \log \frac{1}{-x}, & -\frac{1}{e} < x \le 0, \\ 0, & x = 0, \\ x \log \frac{1}{x}, & 0 < x \le \frac{1}{e}, \\ \frac{1}{e}, & x > \frac{1}{e}. \end{cases}$$

Note that ϕ is a continuous, and concave function, and that $\lim_{x\to 0} \phi(x) = 0$. In addition, we have the following properties for the auxiliary function $\phi(\cdot)$.

Lemma 6. For any $a, b \in [0, 1], |a \log(a) - b \log(b)| \le \phi(a - b).$

Lemma 7. For any real numbers a and b, we have $\phi(a+b) \leq \phi(|a|) + \phi(|b|)$.

I. Bound on
$$\left|\left(\hat{I}(Y;\tilde{T}_1) - \hat{I}(Y;\tilde{T}_1^*)\right)\right|$$
.

Without loss of generality and reduce the complexity, we denote $T \equiv \tilde{T}_1$ and $T^* \equiv \tilde{T}_1^*$. By the triangle inequality, we have:

$$|\hat{I}(Y;T) - \hat{I}(Y;T^*)| \leq \underbrace{|\underline{I(Y;T) - \hat{I}(Y;T)}|}_{A} + \underbrace{|\underline{I(Y;T^*) - \hat{I}(Y;T^*)}|}_{B} + \underbrace{|\underline{I(Y;T) - I(Y;T^*)}|}_{C}.$$

For terms A and B, we have the following bound which is given by the Theorem 2 in the paper (Shamir et al., 2010).

$$\begin{split} |I(Y;T) - \hat{I}(Y;T)| &\leq (2 + \sqrt{2\log((|\mathcal{Y}|+2)/\delta)}) \sqrt{\frac{V(\hat{H}(T|Y))}{M}} \\ &+ 2 \int_{\mathcal{T}} \phi\Bigg((2 + \sqrt{2\log((|\mathcal{Y}|+2)/\delta)}) \sqrt{\frac{V(p(T|X))}{M}}\Bigg) p_T(t) \, dt \\ &\leq (2 + \sqrt{2\log((|\mathcal{Y}|+2)/\delta)}) \sqrt{\frac{V(H(T|Y))}{M}} \\ &+ 2 \int_{\mathcal{T}} \phi\Bigg((2 + \sqrt{2\log((|\mathcal{Y}|+2)/\delta)}) \sqrt{\frac{V(p(T|X))}{M}}\Bigg) p_T(t) \, dt \quad \text{(Law of Large Numbers)} \end{split}$$

B)

$$\begin{split} |I(Y;T^*) - \hat{I}(Y;T^*)| &\leq (2 + \sqrt{2\log((|\mathcal{Y}|+2)/\delta)})\sqrt{\frac{V(\hat{H}(T^*|Y))}{M}} \\ &+ 2\int_{\mathcal{T}^*} \phi\Bigg((2 + \sqrt{2\log((|\mathcal{Y}|+2)/\delta)})\sqrt{\frac{V(p(T^*|X))}{M}}\Bigg) p_{T^*}(t)\,dt \\ &\leq (2 + \sqrt{2\log((|\mathcal{Y}|+2)/\delta)})\sqrt{\frac{V(H(T^*|Y))}{M}} \\ &+ 2\int_{\mathcal{T}^*} \phi\Bigg((2 + \sqrt{2\log((|\mathcal{Y}|+2)/\delta)})\sqrt{\frac{V(p(T^*|X))}{M}}\Bigg) p_{T^*}(t)\,dt \quad \text{(Law of Large Numbers)} \end{split}$$

For term C, we have

C)

$$|I(Y;T) - I(Y;T^*)| \le |H(T|Y) - H(T^*|Y)| + |H(T) - H(T^*)|$$

$$\begin{split} &|H(T|Y) - H(T^*|Y)| = |\sum_{y} p(y) \big(H(T|y) - H(T^*|y) \big)| \\ &= |\sum_{y} p(y) \int_{\mathcal{T}} p_{T|Y}(t|y) \log(p_{T|Y}(t|y)) dt - \sum_{y} p(y) \int_{\mathcal{T}^*} p_{T^*|Y}(t|y) \log(p_{T^*|Y}(t|y)) dt | \\ &\leq \sum_{y} p(y) |\int_{\mathcal{T}} p_{T|Y}(t|y) \log(p_{T|Y}(t|y)) - p_{T^*|Y}(t|y) \log(p_{T^*|Y}(t|y)) dt | \\ &\leq \sum_{y} p(y) \int_{\mathcal{T}} |p_{T|Y}(t|y) \log(p_{T|Y}(t|y)) - p_{T^*|Y}(t|y) \log(p_{T^*|Y}(t|y)) | dt \\ &\leq \sum_{y} p(y) \int_{\mathcal{T}} \phi(p_{T|Y}(t|y) - p_{T^*|Y}(t|y)) dt \quad \text{(By Lemma 6)} \\ &= \sum_{y} p(y) \int_{\mathcal{T}} \phi(p_{T|Y}(t|y) - \mathbb{E}[p_{T|Y}(t|y)] + \mathbb{E}[p_{T|Y}(t|y)] - p_{T^*|Y}(t|y)) dt \\ &\leq \sum_{y} p(y) \int_{\mathcal{T}} \phi(|p_{T|Y}(t|y) - \mathbb{E}[p_{T|Y}(t|y)]) + \phi(|\mathbb{E}[p_{T|Y}(t|y)]|) + \phi(|p_{T^*|Y}(t|y)|) dt \quad \text{(By Lemma 7)} \\ &\leq \sum_{y} p(y) \int_{\mathcal{T}} \phi(\sqrt{V(p_{T|Y}(t|y))}) + \phi(\mathbb{E}[p_{T|Y}(t|y)]) + \phi(p_{T^*|Y}(t|y)) dt \end{split}$$

24

(23)

$$|H(T) - H(T^*)| = |\int_{\mathcal{T}} p_T(t) \log(p_T(t)) dt - \int_{\mathcal{T}^*} p_{T^*}(t) \log(p_{T^*}(t)) dt|$$

$$\leq |\int_{\mathcal{T}} p_T(t) \log(p_T(t)) - p_{T^*}(t) \log(p_{T^*}(t)) dt|$$

$$\leq \int_{\mathcal{T}} \sum_{x} p(x) |p_{T|X}(t|x) \log(p_{T|X}(t|x)) - p_{T^*|X}(t|x) \log(p_{T^*|X}(t|x))| dt \quad \text{(By Lemma 6)}$$

$$\leq \int_{\mathcal{T}} \sum_{x} p(x) \phi(p_{T|X}(t|x) - p_{T^*|X}(t|x)) dt$$

$$\leq \int_{\mathcal{T}} \sum_{x} p(x) [\phi(\sqrt{V(p_{T|X}(t|x))}) + \phi(\mathbb{E}[p_{T|X}(t|x)]) + \phi(p_{T^*|X}(t|x))] dt$$

Combining i) and ii), we have

ii)

$$|\hat{I}(Y;T) - \hat{I}(Y;T^*)| \leq \sum_{y} p(y) \int_{\mathcal{T}} \phi(\sqrt{V(p_{T|Y}(t|y))}) + \phi(\mathbb{E}[p_{T|Y}(t|y)]) + \phi(p_{T^*|Y}(t|y))dt + \int_{\mathcal{T}} \sum_{x} p(x) [\phi(\sqrt{V(p_{T|X}(t|x))}) + \phi(\mathbb{E}[p_{T|X}(t|x)]) + \phi(p_{T^*|X}(t|x))]dt$$
(25)

Thus, in our setting, we have:

$$\begin{split} \left| \left(\hat{I}(Y; \tilde{T}_{1}) - \hat{I}(Y; \tilde{T}_{1}^{*}) \right) \right| &\leq (2 + \sqrt{2 \log((|\mathcal{Y}| + 2)/\delta)}) \sqrt{\frac{V(H(\tilde{T}_{1}|Y))}{M}} \\ &+ 2 \int_{\tilde{T}_{1}} \phi \left((2 + \sqrt{2 \log((|\mathcal{Y}| + 2)/\delta)}) \sqrt{\frac{V(p(\tilde{T}_{1}|X))}{M}} \right) p_{\tilde{T}_{1}}(t) \, dt \\ &+ (2 + \sqrt{2 \log((|\mathcal{Y}| + 2)/\delta)}) \sqrt{\frac{V(H(\tilde{T}_{1}^{*}|Y))}{M}} \\ &+ 2 \int_{\tilde{T}_{1}^{*}} \phi \left((2 + \sqrt{2 \log((|\mathcal{Y}| + 2)/\delta)}) \sqrt{\frac{V(p(\tilde{T}_{1}^{*}|X))}{M}} \right) p_{\tilde{T}_{1}^{*}}(t) \, dt \\ &+ \sum_{y} p(y) \int_{\tilde{T}_{1}} \phi(\sqrt{V(p_{\tilde{T}_{1}|Y}(t|y))}) + \phi(\mathbb{E}[p_{\tilde{T}_{1}|Y}(t|y)]) + \phi(p_{\tilde{T}_{1}^{*}|Y}(t|y)) \, dt \\ &+ \int_{\tilde{T}_{1}} \sum_{z} p(x) [\phi(\sqrt{V(p_{\tilde{T}_{1}|X}(t|x))}) + \phi(\mathbb{E}[p_{\tilde{T}_{1}|X}(t|x)]) + \phi(p_{\tilde{T}_{1}^{*}|X}(t|x))] dt \end{split}$$

II. Bound on
$$\beta \left| \left(\hat{I}(X; \tilde{T}_1) - \hat{I}(X; \tilde{T}_1^*) \right) \right|$$
.

Without loss of generality and reduce the complexity, we denote $T \equiv \tilde{T}_1$ and $T^* \equiv \tilde{T}_1^*$. By the triangle inequality, we have:

$$|\hat{I}(X;T) - \hat{I}(X;T^*)| \leq \underbrace{|I(X;T) - \hat{I}(X;T)|}_{A'} + \underbrace{|I(X;T^*) - \hat{I}(X;T^*)|}_{B'} + \underbrace{|I(X;T) - I(X;T^*)|}_{C'}.$$

For terms A' and B', we have the following bound which is given by the Theorem 2 in the paper (Shamir et al., 2010).

A')

$$|I(X;T) - \hat{I}(X;T)| \le (2 + \sqrt{2\log((|\mathcal{Y}| + 2)/\delta)})\sqrt{\frac{V(H(T|X))}{M}} + \int_{\mathcal{T}} \phi\left((2 + \sqrt{2\log((|\mathcal{Y}| + 2)/\delta)})\sqrt{\frac{V(p(T|X))}{M}}\right) p_T(t) dt,$$

B')

$$|I(X; T^*) - \hat{I}(X; T^*)| \le (2 + \sqrt{2\log((|\mathcal{Y}| + 2)/\delta)}) \sqrt{\frac{V(H(T^*|X))}{M}} + \int_{\mathcal{T}_*} \phi\left((2 + \sqrt{2\log((|\mathcal{Y}| + 2)/\delta)}) \sqrt{\frac{V(p(T^*|X))}{M}}\right) p_{T^*}(t) dt.$$

C')

$$|I(X;T) - I(X;T^*)| \le |H(T|X) - H(T^*|X)| + |H(T) - H(T^*)|$$

As shown in the C) $|I(Y;T) - I(Y;T^*)|$ case, similarly, we have

$$|I(X;T) - I(X;T^*)| \leq \sum_{x} p(x) \int_{\mathcal{T}} \phi(\sqrt{V(p_{T|X}(t|x))}) + \phi(\mathbb{E}[p_{T|X}(t|x)]) + \phi(p_{T^*|X}(t|x))dt + \int_{\mathcal{T}} \sum_{x} p(x) [\phi(\sqrt{V(p_{T|X}(t|x))}) + \phi(\mathbb{E}[p_{T|X}(t|x)]) + \phi(p_{T^*|X}(t|x))]dt$$
(27)

Thus, in our setting, we have

$$\beta \left| \left(\hat{I}(X; \tilde{T}_{l}) - \hat{I}(X; \tilde{T}_{l}^{*}) \right) \right| \leq \beta (2 + \sqrt{2 \log((|\mathcal{Y}| + 2)/\delta)}) \sqrt{\frac{V(H(\tilde{T}_{1}|X))}{M}}$$

$$+ \beta \int_{\tilde{T}_{1}} \phi \left((2 + \sqrt{2 \log((|\mathcal{Y}| + 2)/\delta)}) \sqrt{\frac{V(p(\tilde{T}_{1}|X))}{M}} \right) p_{\tilde{T}_{1}}(t) dt$$

$$+ \beta (2 + \sqrt{2 \log((|\mathcal{Y}| + 2)/\delta)}) \sqrt{\frac{V(H(\tilde{T}_{1}^{*}|X))}{M}}$$

$$+ \beta \int_{\tilde{T}_{1}^{*}} \phi \left((2 + \sqrt{2 \log((|\mathcal{Y}| + 2)/\delta)}) \sqrt{\frac{V(p(\tilde{T}_{1}^{*}|X))}{M}} \right) p_{\tilde{T}_{1}^{*}}(t) dt$$

$$+ \beta \sum_{x} p(x) \int_{\tilde{T}_{1}} \phi(\sqrt{V(p_{\tilde{T}_{1}|X}(t|x))}) + \phi(\mathbb{E}[p_{\tilde{T}_{1}|X}(t|x)]) + \phi(p_{\tilde{T}_{1}^{*}|X}(t|x)) dt$$

$$+ \int_{\tilde{T}_{1}} \sum_{x} p(x) [\phi(\sqrt{V(p_{\tilde{T}_{1}|X}(t|x))}) + \phi(\mathbb{E}[p_{\tilde{T}_{1}|X}(t|x)]) + \phi(p_{\tilde{T}_{1}^{*}|X}(t|x))] dt$$

Combining I and II, we have the bound

$$\begin{split} \Delta_{S}(\tilde{T}_{1};\tilde{T}_{1}^{*}) &\leq \sum_{l=1}^{L} \left((2 + \sqrt{2 \log((|\mathcal{Y}| + 2)/\delta)}) \sqrt{\frac{V(H(\tilde{T}_{1}|Y))}{M}} \right) \\ &+ 2 \int_{\tilde{T}_{1}} \phi \left((2 + \sqrt{2 \log((|\mathcal{Y}| + 2)/\delta)}) \sqrt{\frac{V(p(\tilde{T}_{1}|X))}{M}} \right) p_{\tilde{T}_{1}}(t) \, dt \\ &+ (2 + \sqrt{2 \log((|\mathcal{Y}| + 2)/\delta)}) \sqrt{\frac{V(H(\tilde{T}_{1}^{*}|Y))}{M}} \\ &+ 2 \int_{\tilde{T}_{1}^{*}} \phi \left((2 + \sqrt{2 \log((|\mathcal{Y}| + 2)/\delta)}) \sqrt{\frac{V(p(\tilde{T}_{1}^{*}|X))}{M}} \right) p_{\tilde{T}_{1}^{*}}(t) \, dt \\ &+ \sum_{y} p(y) \int_{\tilde{T}_{1}} \phi(\sqrt{V(p_{\tilde{T}_{1}|Y}(t|y))}) + \phi(\mathbb{E}[p_{\tilde{T}_{1}|Y}(t|y)]) + \phi(p_{\tilde{T}_{1}^{*}|Y}(t|y)) \, dt \\ &+ \beta(2 + \sqrt{2 \log((|\mathcal{Y}| + 2)/\delta)}) \sqrt{\frac{V(H(\tilde{T}_{1}|X))}{M}} \\ &+ \beta \int_{\tilde{T}_{1}^{*}} \phi \left((2 + \sqrt{2 \log((|\mathcal{Y}| + 2)/\delta)}) \sqrt{\frac{V(p(\tilde{T}_{1}|X))}{M}} \right) p_{\tilde{T}_{1}}(t) \, dt \\ &+ \beta(2 + \sqrt{2 \log((|\mathcal{Y}| + 2)/\delta)}) \sqrt{\frac{V(p(\tilde{T}_{1}^{*}|X))}{M}} \\ &+ \beta \int_{\tilde{T}_{1}^{*}} \phi \left((2 + \sqrt{2 \log((|\mathcal{Y}| + 2)/\delta)}) \sqrt{\frac{V(p(\tilde{T}_{1}^{*}|X))}{M}} \right) p_{\tilde{T}_{1}^{*}}(t) \, dt \\ &+ \beta \sum_{x} p(x) \int_{\tilde{T}_{1}^{*}} \phi(\sqrt{V(p_{\tilde{T}_{1}|X}(t|x))}) + \phi(\mathbb{E}[p_{\tilde{T}_{1}|X}(t|x)]) + \phi(p_{\tilde{T}_{1}^{*}|X}(t|x)) \, dt \\ &+ (\beta + 1) \int_{\tilde{T}_{1}^{*}} \sum_{x} p(x) [\phi(\sqrt{V(p_{\tilde{T}_{1}|X}(t|x))}) + \phi(\mathbb{E}[p_{\tilde{T}_{1}|X}(t|x)]) + \phi(p_{\tilde{T}_{1}^{*}|X}(t|x))] dt \end{pmatrix} \end{split}$$

We begin by defining the main functional related to representation \tilde{T}_1 that controls the generalization gap:

$$\begin{split} &G(\sigma_{H_{1}|X},\sigma_{H_{1}|Y},\sigma_{p_{1}|X},\sigma_{p_{1}|Y},\mu_{p_{1}|X},\mu_{p_{1}|Y})\\ &=C_{1}\sqrt{\frac{\sigma_{H_{1}|X}}{M}}+C_{1}\sqrt{\frac{\sigma_{H_{1}|Y}}{M}}+\sum_{y}p(y)\int_{\mathcal{T}_{1}}\phi(\sqrt{\sigma_{p_{1}|Y}})\,dt+\beta\sum_{x}p(x)\int_{\tilde{\mathcal{T}}_{1}}\phi(\sqrt{\sigma_{p_{1}|X}})\,dt\\ &+(\beta+2)\int_{\tilde{\mathcal{T}}_{1}}\phi\Big(C_{1}\sqrt{\frac{\sigma_{H_{1}|X}}{M}}\Big)p_{\tilde{\mathcal{T}}_{1}}(t)\,dt+\sum_{y}p(y)\int_{\tilde{\mathcal{T}}_{1}}\phi(\mu_{p_{1}|Y})\,dt+\beta\sum_{x}p(x)\int_{\tilde{\mathcal{T}}_{1}}\phi(\mu_{p_{1}|X})\,dt\\ &+(\beta+1)\int_{\tilde{\mathcal{T}}_{1}}\sum_{x}p(x)[\phi(\sqrt{\sigma_{p_{1}|X}})+\phi(\mu_{p_{1}|X})]dt, \end{split} \tag{30}$$

where

$$\begin{split} \sigma_{H_1|X} &:= V(H(\tilde{T}_1|X)) = |\mathcal{X}| \mathbb{V}(H(\tilde{T}_1|X)), \quad \sigma_{H_1|Y} := V(H(\tilde{T}_1|Y)) = |\mathcal{Y}| \mathbb{V}(H(\tilde{T}_1|Y)), \\ \sigma_{p_1|X} &:= V(p(\tilde{T}_1|X)) = |\mathcal{X}| \mathbb{V}(p(\tilde{T}_1|X)), \qquad \sigma_{p_1|Y} := V(p(\tilde{T}_1|Y)) = |\mathcal{Y}| \mathbb{V}(p(\tilde{T}_1|Y)), \\ \mu_{p_1|X} &:= \mathbb{E}[p(\tilde{T}_1|X)], \qquad \qquad \mu_{p_1|Y} := \mathbb{E}[p(\tilde{T}_1|Y)], \end{split}$$

and

$$C_1 = 2 + \sqrt{2\log((|\mathcal{Y}| + 2)/\delta)}.$$

 \tilde{T}_1^* should satisfy the self-consistent equations (Tishby et al., 2000):

$$p(\tilde{T}_{1}^{*}|X) = \frac{p(\tilde{T}_{1}^{*})}{Z(\tilde{T}_{0},\beta)} \exp\left[-\beta \sum_{y} p(Y=y|\tilde{T}_{0}) \log \frac{p(Y=y|\tilde{T}_{0})}{p(Y=y|\tilde{T}_{1}^{*})}\right],$$

$$p(Y|\tilde{T}_{1}^{*}) = \frac{1}{p(\tilde{T}_{1}^{*})} \int_{\tilde{\tau}_{0}} p(Y|\tilde{T}_{0}=t) p(\tilde{T}_{1}^{*}|\tilde{T}_{0}=t) p(\tilde{T}_{0}=t) dt,$$

$$p(\tilde{T}_{1}^{*}) = \int_{\tilde{\tau}_{0}} p(\tilde{T}_{1}^{*}|\tilde{T}_{0}=t) p(\tilde{T}_{0}=t) dt$$
(31)

where $Z(\tilde{T}_0^*,\beta)$ is the partition function. Thus, we can write the left terms to optimum–dependent components:

$$\begin{split} Q(\tilde{T}_{1}^{*}) &= (2 + \sqrt{2 \log((|\mathcal{Y}| + 2)/\delta)}) \sqrt{\frac{V(H(\tilde{T}_{1}^{*}|Y))}{M}} \\ &+ \beta (2 + \sqrt{2 \log((|\mathcal{Y}| + 2)/\delta)}) \sqrt{\frac{V(H(\tilde{T}_{1}^{*}|X))}{M}} \\ &+ (\beta + 2) \int_{\tilde{T}_{1}^{*}} \phi \Bigg((2 + \sqrt{2 \log((|\mathcal{Y}| + 2)/\delta)}) \sqrt{\frac{V(p(\tilde{T}_{1}^{*}|X))}{M}} \Bigg) p_{\tilde{T}_{1}^{*}}(t) \, dt \\ &+ \sum_{y} p(y) \int_{\tilde{T}_{1}} \phi(p_{\tilde{T}_{1}^{*}|Y}(t|y)) \, dt + \beta \sum_{x} p(x) \int_{\tilde{T}_{1}} \phi(p_{\tilde{T}_{1}^{*}|X}(t|x)) \, dt + (\beta + 1) \int_{\tilde{T}_{1}} \phi(p(\tilde{T}_{1}^{*})) \, dt \\ &+ (\beta + 1) \int_{\tilde{T}_{1}} \sum_{x} p(x) \phi(p_{\tilde{T}_{1}^{*}|X}(t|x)) dt \quad \text{(By Eqn. (31))} \end{split}$$

Thus, we now can decompose the gap as the following form:

$$\Delta_{S}(\tilde{T}_{1}; \tilde{T}_{1}^{*}) \leq G(\sigma_{H_{1}|X}, \sigma_{H_{1}|Y}, \sigma_{p_{1}|X}, \sigma_{p_{1}|Y}, \mu_{p_{1}|X}, \mu_{p_{1}|Y}) + Q(T_{1}^{*}). \tag{33}$$

E.3 Proof for Proposition 4

Proposition (Entropy Reduction). For any random vector $Z \in \mathbb{R}^d$ with distribution \mathbb{P}_Z , the compression operation s_λ in IBNorm satisfies

$$H(s_{\lambda}(Z)) < H(Z), \tag{34}$$

where $H(\cdot)$ denotes differential entropy.

Proof. Since s_{λ} is measurable and strictly monotone non-decreasing, it is an invertible mapping on its range. Let $J_{s_{\lambda}}(Z)$ denote the Jacobian matrix of s_{λ} .

Using the change-of-variables formula for differential entropy:

$$H(s_{\lambda}(Z)) = H(Z) + \mathbb{E}[\log |\det J_{s_{\lambda}}(Z)|] \leq H(Z),$$

because $|\det J_{s_{\lambda}}(Z)| = \prod_{i=1}^{d} f'_{\lambda}(|Z_{i} - \mu|) \leq \prod_{i=1}^{d} \alpha_{\lambda} \leq 1$ by the bounded compression property of f_{λ} .

Hence, s_{λ} concentrates the distribution and does not increase entropy.

E.4 PROOF FOR LEMMA 5

Lemma. 1) Let $\tilde{T}_{IB} = s_{\lambda}(\tilde{T}_s)$, where s_{λ} is a bounded-compression mapping with Lipschitz constant $L_1 = \prod_{i=1}^d \frac{1}{\lambda}$. For any small $\delta > 0$, the following holds:

$$\mathbb{P}(\mathbb{V}(H(\tilde{T}_{IB}|X)) \leq \mathbb{V}(H(\tilde{T}_{s}|X))) \geq 1 - \delta, \quad \mathbb{P}(\mathbb{V}(H(\tilde{T}_{IB}|Y)) \leq \mathbb{V}(H(\tilde{T}_{s}|Y))) \geq 1 - \delta.$$

2) In addition, let $\tilde{T}_1, \tilde{T}'_1 \in \tilde{T}_1$ be two arbitrary elements in the representation space. Then, for any $\delta \in (0,1)$, the following holds with probability at least $1-\delta$:

$$\begin{split} &|\mathbb{V}(p(\tilde{T}_1|X)) - \mathbb{V}(p(\tilde{T}_1'|X))| \leq \delta, \\ &|\mathbb{V}(p(\tilde{T}_1|Y)) - \mathbb{V}(p(\tilde{T}_1'|Y))| \leq \delta, \\ &|\mathbb{E}[p(\tilde{T}_1|X)] - \mathbb{E}[p(\tilde{T}_1'|X)]| \leq \delta, \\ &|\mathbb{E}[p(\tilde{T}_1|Y)] - \mathbb{E}[p(\tilde{T}_1'|Y)]| \leq \delta, \end{split}$$

where the expectation and variance are taken with respect to the Lebesgue measure on $\mathcal{X} \times \mathcal{Y}$.

Proof. 1) We first prove the first part of the Lemma.

We consider the two representations:

$$\tilde{T}_s = \Phi_s(X') = \eta \circ \psi_s \circ \zeta(X'), \qquad \tilde{T}_{IB} = \Phi_{IB}(X') = \eta \circ \psi_{IB} \circ \zeta(X'),$$

where X' = h(X), $\psi_{IB} = \psi_s \circ s_\lambda$ with s_λ being the compression operation in IBNorm.

From the Proposition 4, we have for any fixed input Z:

$$H(\psi_{\mathrm{IB}}(Z)) = H(s_{\lambda}(\psi_{\mathrm{s}}(Z))) \le H(\psi_{\mathrm{s}}(Z)).$$

Thus, the conditional entropy of \tilde{T}_{IB} is pointwise bounded by that of \tilde{T}_s .

Applying this to the conditional distributions $\tilde{T}_{IB}|X$ and $\tilde{T}_{s}|X$, we get:

$$H(\tilde{T}_{IB}|X) \le H(\tilde{T}_s|X), \qquad H(\tilde{T}_{IB}|Y) \le H(\tilde{T}_s|Y).$$

If we consider the entropy H in the discrete case, we can directly derive the relationship: consider the conditional entropy as a random variable over X (or Y). Let $f'(Z) := H(s_{\lambda}(Z))$, then:

- 1. s_{λ} is a Lipschitz map with Lipschitz constant $L \leq 1$ because $|\det J_{s_{\lambda}}(Z)| = \prod_{i=1}^{d} f'_{\lambda}(|Z_i \mu|) \leq \prod_{i=1}^{d} \alpha_{\lambda} \leq 1$ by the bounded compression property of f_{λ} .
- 2. $H(\cdot)$ is 1-Lipschitz continuous on the space of probability distributions bounded away from zero.

Hence, $f'(\tilde{T}_s|X)$ is a Lipschitz transformation of $\tilde{T}_s|X$, implying by standard variance contraction results:

$$\mathbb{V}(H(\tilde{T}_{IB}|X)) = \mathbb{V}(f'(\tilde{T}_s|X)) \le L^2 \mathbb{V}(H(\tilde{T}_s|X)) \le \mathbb{V}(H(\tilde{T}_s|X)).$$

Similarly,

$$\mathbb{V}(H(\tilde{T}_{IB}|Y)) \leq \mathbb{V}(H(\tilde{T}_{s}|Y)).$$

In the differential entropy case, we cannot guarantee a global Lipschitz constant L < 1 for $f'(\tilde{T}_s|X) = H(\tilde{T}_s|X) + \Delta'(\tilde{T}_s|X)$. Instead, we proceed in a high-probability setting.

For any $\delta > 0$, let

$$\mathcal{T}^s_{\delta} := \{ t \in \mathbb{R}^d : m_{\delta} \le p_{\tilde{T}_s|X=x}(t) \le M_{\delta} \}, \quad \mathbb{P}(\tilde{T}_s \in \mathcal{T}^s_{\delta}) \ge 1 - \delta,$$

where $0 < m_{\delta} < M_{\delta} < \infty$. By construction, \mathcal{T}_{δ}^{s} is bounded: $\exists a,b \in \mathbb{R}, \quad s.t.\mathcal{T}_{\delta}^{s} \subset [a,b]^{d}$. This ensures that the conditional density is bounded away from zero and infinity on the high-probability set.

Let $\tilde{T}_{IB} = s_{\lambda}(\tilde{T}_s)$, with s_{λ} differentiable and invertible. Then the conditional density transforms as

$$p_{\tilde{T}_{IB}|X=x}(t) = p_{\tilde{T}_s|X=x}(s_{\lambda}^{-1}(t)) \, |\det J_{s_{\lambda}^{-1}}(t)|,$$

where $J_{s_{\lambda}}$ is the Jacobian of s_{λ} . The conditional differential entropy is

$$H(\tilde{T}_{IB}|X=x) = H(\tilde{T}_s|X=x) + \Delta(\tilde{T}_s), \quad \Delta(\tilde{T}_s) := \log|\det J_{s_\lambda}(\tilde{T}_s)|.$$

Since s_{λ} has bounded derivatives, for any $t_1, t_2 \in \mathcal{T}_{\delta}^s$,

$$|\Delta(t_1) - \Delta(t_2)| \le L_1 ||t_1 - t_2||,$$

for the constant $L_1 = \prod_{i=1}^d \alpha_{\lambda} = \prod_{i=1}^d \frac{1}{\lambda}$ determined by the bounds of the Jacobian of s_{λ} .

For any two conditional densities p_1, p_2 of $\tilde{T}_s|X$ supported in \mathcal{T}_{δ}^s , standard results for differential entropy bounded away from zero and infinity imply

$$|H(p_1) - H(p_2)| \le L_2 ||p_1 - p_2||_1$$

with $L_2 := |\log m_{\delta}| + 1/m_{\delta}$. Hence $H(\tilde{T}_s|X)$ is Lipschitz on \mathcal{T}_{δ}^s .

For $\tilde{T}_s \in \mathcal{T}^s_{\delta}$, we have

$$\mathbb{V}(H(\tilde{T}_{IB}|X) \mid \tilde{T}_s \in \mathcal{T}^s_{\delta}) = \mathbb{V}(H(\tilde{T}_s|X) + \Delta(\tilde{T}_s) \mid \tilde{T}_s \in \mathcal{T}^s_{\delta}).$$

Expanding using the variance formula,

$$\mathbb{V}(H(\tilde{T}_s|X) + \Delta(\tilde{T}_s)) = \mathbb{V}(H(\tilde{T}_s|X)) + \mathbb{V}(\Delta(\tilde{T}_s)) + 2\operatorname{Cov}(H(\tilde{T}_s|X), \Delta(\tilde{T}_s)).$$

Since $\Delta(\tilde{T}_s)$ is Lipschitz with constant L_1 on the bounded set $\mathcal{T}_{\delta}^s \subset [a,b]^d$, we have

$$\mathbb{V}(\Delta(\tilde{T}_s) \mid \tilde{T}_s \in \mathcal{T}_{\delta}^s) \le \frac{1}{4}L_1^2(b-a)^2.$$

Moreover, under the bounded-compression property of s_{λ} , the covariance term is non-positive:

$$Cov(H(\tilde{T}_s|X), \Delta(\tilde{T}_s) \mid \tilde{T}_s \in \mathcal{T}_{\delta}^s) \leq 0.$$

Remark. The covariance term $\operatorname{Cov}(H(\tilde{T}_s|X), \Delta(\tilde{T}_s))$ is typically negative because, under the bounded-compression property of s_{λ} , larger conditional entropy $H(\tilde{T}_s|X)$ corresponds to a more spread-out distribution, which is locally contracted more by s_{λ} , resulting in smaller $\Delta(\tilde{T}_s) = \log |\det J_{s_{\lambda}}(\tilde{T}_s)|$. On the high-probability set \mathcal{T}_{δ}^s , any residual covariance can be made arbitrarily small by choosing δ sufficiently small.

Combining these terms, we obtain a high-probability variance contraction:

$$\mathbb{V}(H(\tilde{T}_{IB}|X) \mid \tilde{T}_s \in \mathcal{T}_{\delta}^s) \le \mathbb{V}(H(\tilde{T}_s|X) \mid \tilde{T}_s \in \mathcal{T}_{\delta}^s) + \frac{1}{4}L_1^2(b-a)^2.$$

Similarly, for Y.

$$\mathbb{V}(H(\tilde{T}_{IB}|Y) \mid \tilde{T}_s \in \mathcal{T}_{\delta}^s) \le \mathbb{V}(H(\tilde{T}_s|Y) \mid \tilde{T}_s \in \mathcal{T}_{\delta}^s) + \frac{1}{4}L_1^2(b-a)^2,$$

where $L_1 = \prod_{i=1}^d \frac{1}{\lambda}$.

We can always choose $\lambda > 1$ sufficiently large so that the Lipschitz constant $L_1 = \prod_{i=1}^d \frac{1}{\lambda}$ is small enough to ensure $\frac{1}{4}L_1^2(b-a)^2 + 2\mathrm{Cov}(H(\tilde{T}_s|X),\Delta(\tilde{T}_s)\mid \tilde{T}_s\in\mathcal{T}_\delta^s) \leq 0$. Consequently, we obtain

$$\mathbb{V}(H(\tilde{T}_{IB}|X) \mid \tilde{T}_s \in \mathcal{T}^s_{\delta}) \leq \mathbb{V}(H(\tilde{T}_s|X) \mid \tilde{T}_s \in \mathcal{T}^s_{\delta}),$$

and

$$\mathbb{V}(H(\tilde{T}_{IB}|Y) \mid \tilde{T}_s \in \mathcal{T}_{\delta}^s) \leq \mathbb{V}(H(\tilde{T}_s|Y) \mid \tilde{T}_s \in \mathcal{T}_{\delta}^s).$$

Finally, taking into account that $\mathbb{P}(\tilde{T}_s \in \mathcal{T}_{\delta}^s) \geq 1 - \delta$ and letting $\delta \to 0$, we have that, for any small $\delta > 0$, the following holds:

$$\mathbb{P}(\mathbb{V}(H(\tilde{T}_{IB}|X)) \leq \mathbb{V}(H(\tilde{T}_{s}|X))) \geq 1 - \delta, \quad \mathbb{P}(\mathbb{V}(H(\tilde{T}_{IB}|Y)) \leq \mathbb{V}(H(\tilde{T}_{s}|Y))) \geq 1 - \delta.$$

2) We then prove the second part of the Lemma.

Lemma 8. Given the compact representation space \tilde{T}_1 , for any $\delta > 0$, there exists $\epsilon > 0$ such that

$$\|\tilde{T}_1 - \tilde{T}_1'\| < \epsilon \implies |p(\tilde{T}_1|X) - p(\tilde{T}_1'|X)| < \delta/2, \quad |p(\tilde{T}_1|Y) - p(\tilde{T}_1'|Y)| < \delta/2.$$

Lemma 9. For any bounded functions $f, g : \mathcal{X} \to \mathbb{R}$,

$$|\mathbb{E}[f] - \mathbb{E}[g]| \le ||f - g||_{\infty}, \quad |\mathbb{V}(f) - \mathbb{V}(g)| \le ||f - g||_{\infty} \left(2\sqrt{\mathbb{V}(f)} + ||f - g||_{\infty}\right).$$

By Lemma 8, for any $\delta>0$, there exists $\epsilon>0$ such that if $\|\tilde{T}_1-\tilde{T}_1'\|<\epsilon$:

$$|p(\tilde{T}_1|X) - p(\tilde{T}'_1|X)| < \delta/2, \quad |p(\tilde{T}_1|Y) - p(\tilde{T}'_1|Y)| < \delta/2.$$

By Lemma 9, this implies

$$\begin{split} &|\mathbb{E}[p(\tilde{T}_1|X)] - \mathbb{E}[p(\tilde{T}_1'|X)]| \leq \delta, \quad |\mathbb{E}[p(\tilde{T}_1|Y)] - \mathbb{E}[p(\tilde{T}_1'|Y)]| \leq \delta, \\ &|\mathbb{V}(p(\tilde{T}_1|X)) - \mathbb{V}(p(\tilde{T}_1'|X))| \leq \delta, \quad |\mathbb{V}(p(\tilde{T}_1|Y)) - \mathbb{V}(p(\tilde{T}_1'|Y))| \leq \delta. \end{split}$$

Since $\tilde{T}_1, \tilde{T}'_1$ are independently drawn from a measure with full support on the compact set $\tilde{\mathcal{T}}_1$, $\|\tilde{T}_1 - \tilde{T}'_1\| < \epsilon$ holds with probability at least $1 - \delta$.

E.5 PROOF FOR COROLLARY 2

Corollary. With probability at least $1 - \delta$ over training set S of size M, the generalization error of a network f_o satisfies

$$gen(S; f_o) \leq U_o := \sum_{l=1}^L U_l^o, \text{ with } U_l = \sqrt{\frac{I(X; \tilde{T}_l^o|Y) + C(S, f_o) + \log(\frac{2}{\delta})}{M}},$$

where \tilde{T}_l^o is the intermediate representation at layer l before normalization representation recovery η and $C(S, f_o)$ is a term depending on the network f_o and the training set S. Here f_o can be the network f_S using standard normalization like LN and BN, or our network f_{IB} with our IBNorm.

Proof. Theorem 2 in (Kawaguchi et al., 2023) states that, for any $\delta > 0$, with probability at least $1 - \delta$ over the training set S, the following generalization bound holds:

$$\mathrm{gen}(S;f_{\mathrm{o}}) \ \leq \ U_{\mathrm{o}} := \sum\nolimits_{l=1}^{L} U_{l}^{\mathrm{o}}, \ \ \mathrm{with} \ \ U_{l} = \mathcal{O}\Big(\sqrt{\frac{I(X;\tilde{T}_{l}^{\mathrm{o}}|Y) + C(S,f_{\mathrm{o}})}{M}}\Big),$$

where \tilde{T}_l is the intermediate representation at layer l before normalization representation recovery η and $C(S, f_o)$ is a term depending on the network f_o and the training set S. Based on this theorem, we can derive a mutual information related bound as shown in Corollary 2.

Remark. In our experiments, all models are trained on the same dataset, so any dataset-dependent contribution to the generalization bound can be treated as invariant across different normalization schemes. Although the output weight of f_0 during the training process can be thought as a random variable, their information content can be controlled in the training configuration, for instance by injecting noise drawn from a chosen distribution, with variance modulated from zero (allowing, in theory, full memorization of the training set) to a level large enough that no information remains (Achille & Soatto, 2018). Hence, we focus the role of normalization in our analysis: we examine how it shapes the information content of the intermediate representations and thereby affects generalization.

F EXPERIMENTAL DETAILS

F.1 LLM EXPERIMENTS

For all LLaMA models, we follow the setup in (Zhao et al., 2024) and pretrain the vanilla LLaMA series models from scratch on the C4 dataset. We set the maximum input sequence length to 512 and output sequence length to 256, and adopt the bfloat16 precision. For the LLaMA-60M model, we use a learning rate of 0.001, mini-batch size of 64 with gradient accumulation to a global batch size of 512, 20,000 training steps with 1,000 warm-up steps, and the AdamW (Kinga et al., 2015; Loshchilov & Hutter, 2017) optimizer with $(\beta_1, \beta_2) = (0.9, 0.999)$. For the LLaMA-130M model, we use the same learning rate but reduce the mini-batch size to 32 with gradient accumulation to a global batch size of 512, train for 20,000 steps with 2,000 warm-up steps, and maintain the same optimizer configuration. For the LLaMA-350M model, we set the mini-batch size to 16 with gradient accumulation to a global batch size of 512, extend training to 60,000 steps with 6,000 warm-up steps. For the LLaMA-1B model, we set the mini-batch size to 16 with gradient accumulation to a global batch size of 512, extend training to 100,000 steps with 10,000 warm-up steps.

For the GPT-2 series, we follow the Sophia setup (Liu et al., 2023) with the nanoGPT implementation (Karpathy, 2022) and pretrain the vanilla GPT-2 series on OpenWebText (Gokaslan & Cohen, 2019). We set the maximum input sequence length to 1024 and adopt the bfloat16 precision. We use a global batch size of 480, cosine learning rate decay with 2,000 warm-up iterations, and global gradient clipping with a threshold of 1.0. All models are trained for 100,000 steps. We employ the AdamW optimizer with $(\beta_1, \beta_2) = (0.9, 0.95)$ and weight decay of 0.1. For GPT-2 Small (124M), We use a per-device mini-batch size of 12 and 10 gradient accumulation steps across 4 GPUs, resulting in an effective global batch size of 480. We employ a cosine learning rate scheduler with a peak learning rate of 0.0006 and a minimum learning rate of 0.00003. For GPT-2 Medium (355M), we use a per-device mini-batch size of 10 and 12 gradient accumulation steps across 4 GPUs, resulting in an effective global batch size of 480. We employ a cosine learning rate scheduler with a peak learning rate of 0.0003 and a minimum learning rate of 0.0006.

For the hyperparameter noise factor in NormalNorm, we perform a lightweight Sobol-based search on the interval [0,1], and set the value to 1 for all experiments. For the hyperparameter λ in each variant of IBNorm, we conduct a grid search over the set $\{2,3,4,5\}$. The final configurations are $\lambda=3$ for IBNorm-S, and $\lambda=4$ for both IBNorm-L and IBNorm-T. We investigated several hyperparameter configurations, including learning rate, learning rate scheduler, weight decay, and minibatch size, across all models and found the present configurations to generally work best.

All models are trained on 4xNVIDIA L40-S. The total GPU training hours are about 10500 hours for all of our LLM pretraining tasks.

F.2 VISION EXPERIMENTS

ResNet Experiments. In all experiments involving ResNet18 on CIFAR-10, we use stochastic gradient descent (SGD) with learning rate 0.1, weight decay 0.0005, momentum 0.9, and batch size 128 for LayerNorm and NormalNorm, with a noise factor of 0.4. For IBNorm experiments, we use learning rate 0.05 and weight decay 0.001. Following Eftekhari & Papyan (2025), models were trained from random initialization for 200 epochs, with a StepLR scheduler reducing the learning rate by a factor of 10 every 60 epochs.

For experiments with ResNet-50 on ImageNet, a batch size of 256 was used, with SGD parameters: learning rate 0.1, momentum 0.9, Nesterov acceleration enabled, and weight decay 0.0001, along with a cosine annealing learning rate scheduler with maximum 200 epochs and minimum learning rate 0.000001 for BatchNorm and NormalNorm, with a noise factor of 1. For IBNorm experiments, we use learning rate 0.01 and weight decay 0.001. For the hyperparameter λ in each variant of IBNorm, we conduct a grid search over the set $\{2,3,4,5\}$. The final configurations are $\lambda=3$ for IBNorm-S, and $\lambda=4$ for both IBNorm-L and IBNorm-T. We explored several hyperparameter configurations, including learning rate, learning rate scheduler, weight decay, and minibatch size, across all models and found the present configurations to generally work best.

ViT Experiments. We train ViT-S/16 and ViT-B/16 (Dosovitskiy et al., 2020) following the setup (Yuan et al., 2021) on ImageNet. All models are trained for 300 epochs with a global batch size of 512. For ViT-S/16, we use the AdamW optimizer with a learning rate of 0.001, weight decay of 0.03, and $(\beta_1, \beta_2) = (0.9, 0.999)$. For ViT-B/16, the AdamW optimizer is used with a learning rate of 0.001, weight decay of 0.05, and $(\beta_1, \beta_2) = (0.9, 0.999)$. We adopt a hybrid learning rate schedule that combines linear warmup with cosine annealing over the first 10 training epochs. During warmup, the learning rate increases linearly from 0.000001 to the base learning rate. After warmup, cosine annealing is applied for the remaining epochs, gradually decaying the learning rate to a minimum of 0.00001.

We also follow the setup in NormalNorm (Eftekhari & Papyan, 2025) to train a ViT model with 8 transformer layers, 8 attention heads, hidden dimension size 768, MLP dimension size 2304, and patch size 16. Models were trained on ImageNet for 200 epochs with a global batch size of 512. Weighted random sampling based on inverse class frequency was applied during training to improve performance across all model configurations. The AdamW optimizer was used with learning rate 0.001, weight decay 0.05, $(\beta_1, \beta_2) = (0.9, 0.999)$, and epsilon 0.00000001 for LayerNorm, RMSNorm, and NormalNorm, with a noise factor of 1. For IBNorm, we set the learning rate as 0.0002. In addition, we employ a hybrid scheduling strategy that combines linear warmup with cosine annealing over 5 warmup training epochs. During the warmup phase, the learning rate in-

creases linearly from 0.1 to 1.0 of the base learning rate. After warmup, a cosine annealing schedule is applied for the remaining epochs, with the learning rate decaying towards a minimum value of 0.000001.

For the hyperparameter λ in each variant of IBNorm, we conduct a grid search over the set $\{2,3,4,5\}$. The final configurations are $\lambda=3$ for IBNorm-S, and $\lambda=4$ for both IBNorm-L and IBNorm-T. Hyperparameter configurations, including learning rate, scheduler, weight decay, and minibatch size, were explored, and the configurations reported here were found to work best across all ViT models.

All models were trained on 4xNVIDIA L40-S, RTX 3090, and Tesla V100, with a total of approximately 6500 GPU hours for all vision tasks.

G MATHEMATICAL DETAILS FOR MATRIX-BASED INFORMATION ESTIMATION

Following the approach in (Chang et al., 2025), we employ matrix-based Rényi entropy (Giraldo et al., 2014) to estimate mutual information (MI) between model representations and target labels. This method captures sample similarity structures via kernel Gram matrices.

G.1 MATRIX-BASED ENTROPY ESTIMATION

Let $U=\{u_i\}_{i=1}^N$ denote l_2 -normalized representations obtained after the normalization layer. A Gaussian kernel Gram matrix $G_U \in \mathbb{R}^{N \times N}$ is constructed as:

$$(G_U)_{i,j} = \exp\left(-\frac{\|u_i - u_j\|^2}{2\sigma^2}\right),$$

with bandwidth $\sigma = 1$. The matrix is then trace-normalized to ensure $tr(G_U) = 1$.

The matrix-based Rényi entropy of order $\alpha = 1$ is defined as:

$$H(U) = -\operatorname{tr}(G_U \log G_U).$$

This expression can be interpreted in terms of the eigenvalue spectrum $\{\lambda_k\}_{k=1}^N$ of G_U , since G_U is positive semi-definite and trace-normalized:

$$H(U) = \sum_{k=1}^{N} \lambda_k \log \lambda_k.$$

Intuitively, a more uniform eigenvalue spectrum corresponds to higher entropy (more diverse representations), while a sharply peaked spectrum indicates redundancy or compression.

G.2 MUTUAL INFORMATION ESTIMATION

To estimate the mutual information between two random variables U and V, we compute their Gram matrices G_U and G_V , and form the joint similarity matrix via element-wise (Hadamard) product:

$$G_{UV} = G_U \circ G_V.$$

After trace-normalization, mutual information is estimated by:

$$I(U; V) = H(U) + H(V) - H(U, V).$$

where $H(U, V) = -\text{tr}(G_{UV} \log G_{UV})$. A more concentrated eigenvalue spectrum of G_{UV} relative to G_U and G_V indicates stronger dependence between U and V, and thus higher mutual information.

Here we demonstrate our algorithm for calculating the token-level IB value. We consider a transformer model f with L layers. Given an input sequence $x_{1:T}$ of length T, $t_i^{(l)} \in \mathbb{R}^d$ denotes the hidden activation at the last token position of the i-th input sequence after l-th normalization layer, for $l \in [L]$. For next-token prediction, the ground-truth label is denoted by $y_i \in \mathbb{R}^d$, corresponding

to the embedding of the true next token from the vocabulary \mathcal{V} . At a generation time step p and cross a batch of N sequences, we collect the representations:

$$T_{l-1} = \{t_i^{(l-1)}\}_{i=1}^N, T_l = \{t_i^{(l)}\}_{i=1}^N, Y = \{y_i\}_{i=1}^N,$$

where $T_0^{(l)}$ is consisted of the batch of last input tokens x_T hidden representations. We iteratively derive those embeddings: In the first forward pass, a batch of N input sequences $x_{1:T}$ is fed into the transformer to obtain hidden states at each layer. From these, we extract the final-token representations $T_l, l \in [L]$. In the second forward pass, each input is concatenated with its ground-truth next token y, and we extract the corresponding label embedding Y from the output of the embedding layer (Chang et al., 2025). Based on these sets, we can compute two information-theoretic quantities: $I_p(Y,T_l)$ and $I_p(T_l-1,T_l)$ at generation timestep t across $l \in [L]$ and aim to derive the total IB value in the network f given in Eqn. (5), as $\mathbb{E}_p[I_p(Y,T_l)] = \hat{I}(Y,T_l)$ and $\mathbb{E}_p[I_p(T_l-1,T_l)] = \hat{I}(T_l-1,T_l)$ by the Monte Carlo approximation.

In practice, we set the batch size to N=64 and iteratively compute the mutual information values during autoregressive generation until all instances reach the end-of-sequence (< EOS>) token. During autoregressive generation in LLM tasks, different instances in a batch may terminate at different time steps upon reaching the < EOS> token. To handle this, we use a diagonal mask matrix:

$$M \in \{0,1\}^{N \times N}, \quad M_{ii} = \begin{cases} 1, & \text{if instance } i \text{ is still active (not} < EOS >) \\ 0, & \text{if instance } i \text{ has reached} < EOS > \end{cases}.$$

For example, at each step of the generation, the masked Gram matrix for the latent embedding T_l is computed as $\tilde{G}_{T_l} = MG_{T_l}M$ and then conducted trace-normalization.

G.3 TOKEN-LEVEL IB VALUE ESTIMATION

We apply the matrix-based framework to estimate mutual information for token-level IB analysis. Specifically, we uniformly sample P=30 timesteps across the generation process. For each sampled timestep and each layer $l\in [L]$, we extract the representations T_l and compute the following information-theoretic quantities: $I_p(Y,T_l)$ and $I_p(T_l-1,T_l)$ across $l\in [L]$ at sampled timestep t. Then we sum the IB value across l and derive $\sum_{p=1}^P \sum_{l=1}^L \left(I_p(Y;T_l) - \beta I_p(T_{l-1};T_l)\right)$ (we always set $\beta=1$). Finally, the token-level IB value is obtained by averaging over the batch size N and the number of sampled timesteps P.